University of Miami
Scholarly Repository

2012-10-26

Acoustic Emission in Structural Health Monitoring of Reinforced Concrete Structures

Matteo Di Benedetti
University of Miami, teo.dibe@hotmail.it

Follow this and additional works at: https://scholarlyrepository.miami.edu/oa_dissertations

UNIVERSITY OF MIAMI

ACOUSTIC EMISSION IN STRUCTURAL HEALTH MONITORING OF
REINFORCED CONCRETE STRUCTURES

By

Matteo Di Benedetti

A DISSERTATION

Submitted to the Faculty
of the University of Miami
in partial fulfillment of the requirements for
the degree of Doctor of Philosophy

Coral Gables, Florida

December 2012

UNIVERSITY OF MIAMI

A thesis submitted in partial fulfillment of
the requirements for the degree of
Doctor of Philosophy

ACOUSTIC EMISSION IN STRUCTURAL HEALTH MONITORING OF
REINFORCED CONCRETE STRUCTURES

Matteo Di Benedetti

Approved:

_____
Antonio Nanni, Ph.D.
Professor and Chair
of Civil, Architectural,
and Environmental Engineering

_____
M. Brian Blake, Ph.D.
Dean of the Graduate School

_____
Carol Hays, Ph.D.
Associate Professor
of Civil, Architectural,
and Environmental Engineering

_____
Wimal Suaris, Ph.D.
Associate Professor
of Civil, Architectural,
and Environmental Engineering

_____
Marcello Vanali, Ph.D.
Associate Professor
of Industrial Engineering,
Universitá degli Studi di Parma

_____
Fabio Matta, Ph.D.
Assistant Professor of Civil
and Environmental Engineering
University of South Carolina

DI BENEDETTI, MATTEO   (Ph.D., Civil Engineering)
<u>Acoustic Emission in</u>   (December 2012)
<u>Structural Health Monitoring of</u>
<u>Reinforced Concrete Structures.</u>

Abstract of a dissertation at the University of Miami.

Dissertation supervised by Professor Antonio Nanni.
No. of pages in text. (93)

Structural health monitoring (SHM) is a term used in the last decades to describe a range of systems implemented on constructed facilities (including reinforced concrete (RC)) with the purpose of assisting and informing owners/operators on the condition of structures under gradual or sudden changes to their state of serviceability. At the simplest level and with reference to RC, recurrent visual observation and assessment of structural condition (e.g., corrosion, cracking, spalling and deformations) could be viewed as SHM activities. Nowadays, the aim of research efforts is to develop effective and reliable means of acquiring, managing, integrating and interpreting structural performance data. By taking full advantage of the progress in modern technologies, there is an untapped potential to make the assessment of existing RC structures more accurate and cost efficient.

Among the various nondestructive techniques (NDT), acoustic emission (AE) monitoring is arguably based on the simplest physical concepts (nearly everyone has heard audible AE in the form of popping and cracking noises from materials under stress), but is one of the most difficult techniques to practically implement. A formal definition of the AE phenomenon is often given as the release of transient elastic waves in solids as a result of rapid localized redistributions of stresses which accompany the occurrence of damage mechanisms. Examples of AE events related to civil engineering materials include

yielding of steel, crack growth in steel and concrete, corrosion for metals, fiber breakage, and matrix debonding for composites. In this dissertation, AE technology is applied to RC members in order to identify and evaluate damage.

The dissertation is articulated into three studies. The first and the second study (Study 1 and Study 2) focus on the identification of damage and more specifically in the detection of the onset of corrosion by means of AE. The last study (Study 3) presents an innovative AE methodology to assess damage in RC members during load testing.

Study 1 describes the AE monitoring of an experimental campaign on small-scale RC specimens under accelerated corrosion. This study was conducted to investigate the effectiveness of an alternative AE monitoring approach to detect the onset of corrosion that is well suited to the low power requirements typical of long-term detection in the field. Results show that the proposed AE approach, coupled with well-established electrochemical techniques, is a promising tool to develop an early warning alarm system for corrosion in RC structures.

Based on the experience gained in Study 1, Study 2 presents laboratory tests on a second batch of small-scale RC specimens monitored with AE while the corrosion process is accelerated without imposed current. This study was conducted to investigate frequency spectrum of the AE signals before and after onset of corrosion. Results show that the breakage of the protective layer of reinforcing steel, and thus the onset of corrosion, can be localized to a small portion of the AE frequency spectrum.

In Study 3 two identical strips of the one-way RC slab of the first floor of a building scheduled for demolition were saw-cut and load tested. In parallel to the well-established

measurements of load and deflection, an AE monitoring system was implemented. The results demonstrate the suitability of AE technology for assessing damage in the practice of in situ load testing. In particular, AE intensity analysis can be used as a graphical acceptance criterion.

To my Family

TABLE OF CONTENTS

Page

Chapter

Appendices

LIST OF TABLES

LIST OF FIGURES

vi

viii

CHAPTER 1: INTRODUCTION

The term structural health monitoring (SHM) usually refers to the process of implementing a damage detection strategy for aerospace, civil or mechanical engineering structures. This process involves the observation of a structure or mechanical system over time using periodically spaced dynamic response measurements, the extraction of damage-sensitive features from these measurements, and the statistical analysis of these features to determine the current state of system health. For long-term SHM, the output of this process is periodically updated information regarding the ability of the structure to continue to perform its intended function in light of the inevitable aging and degradation resulting from the operational environments. Under an extreme event, such as an earthquake or unanticipated blast loading, SHM could be used for rapid condition screening, to provide, in near real time, reliable information about the performance of the system during the event and about the subsequent integrity of the system.

The majority of the US highway infrastructure was constructed in the 1950-70's with a 50-year design life. The American Society of Civil Engineers (ASCE) estimates that more than 26% of the nation's highway bridges are either structurally deficient or functionally obsolete (ASCE 2009). While some progress has been made in recent years to reduce the number of deficient and obsolete bridges, routine inspection practices are not sufficient for the timely identification of areas of concern and do not provide sufficient information to bridge owners to make informed decisions on safety and maintenance prioritization. Continuous monitoring is needed for long-term evaluation of areas of concern, such as retrofits and previous repairs, or area with known flaws.

Nowadays the aim of research efforts is to develop effective and reliable means of acquiring, managing, integrating and interpreting structural performance data. By taking full advantage of the progress in modern technologies, there is an untapped potential to make the assessment of existing RC members more accurate and cost efficient.

Acoustic emission (AE) testing is an important method within the broad field of nondestructive evaluation techniques (NDE). The term "acoustic emission" is commonly used to describe both a technique and the phenomenon upon which the technique is based. An AE phenomenon consists in the release of transient elastic waves in solids as a result of rapid localized redistributions of stresses (ASTM E1316 2010). The AE monitoring technique uses one or more sensors to 'listen' to a wide range of events that may take place inside a solid material. Examples of AE events related to civil engineering materials include yielding of steel, crack growth in steel and concrete, corrosion of metals, fiber breakage and matrix debonding for composites.

The research of this dissertation is an attempt to improve the existing AE methodology in identifying and evaluating damage in RC members. The dissertation is articulated in three studies. The first two studies present laboratory experiments where AE is employed to monitor small-scale RC specimens under accelerated corrosion. Study 1 investigates the effectiveness of a novel AE monitoring approach to detect the onset of corrosion that is well suited to the low power requirements typical of long-term detection in the field. Study 2 presents the analysis of the frequency spectrum of the AE signals before and after onset of corrosion in order to isolate the frequency components of the corrosion of steel reinforcement. Study 3 focuses on the evaluation of damage in RC members with AE. Two identical strips of the one-way RC slab of the first floor of a building, scheduled

for demolition, were saw-cut and load tested. In parallel to the well-established measurements of load and deflection, an AE monitoring system was implemented in order to define an alternative damage assessment methodology with associated acceptance criteria.

CHAPTER 2: STUDY 1 - ACOUSTIC EMISSION MONITORING OF REINFORCED CONCRETE UNDER ACCELERATED CORROSION

Summary

The development of techniques capable of evaluating the deterioration of reinforced concrete (RC) structures is instrumental to the advancement of structural health monitoring (SHM) techniques and service life estimate methodologies for constructed facilities. One of the main causes leading to degradation of RC structures is the corrosion of steel reinforcement. This process can be modeled phenomenologically, while laboratory tests aimed at studying durability responses are typically accelerated to provide usable results within a realistic period of time. A number of nondestructive methods have been recently studied. Acoustic emission (AE) is emerging as a nondestructive tool to detect the onset and progression of deterioration mechanisms associated with concrete cracking. In Study 1, an accelerated corrosion and AE monitoring test setup is presented, providing relevant information on the characteristics of the corrosion circuit, continuous measurement procedure, selection of AE sensors and AE parameter setting for data acquisition. The effectiveness of AE in detecting and characterizing the initiation of the corrosion process is discussed on the basis of results from small-scale, pre-cracked RC specimens that are representative of areas near the clear cover in typical RC members. The main outcome is a new approach of AE data interpretation based on time-driven (TDD) parameters.

Background

The majority of the US transportation infrastructure (highways and bridges) was constructed in the 1950-70's with a 50-year design life. The American Society of Civil engineers estimates that more than 26% of the nation's bridges are either structurally deficient or functionally obsolete. While some progress has been made in recent years to reduce the number of deficient and obsolete bridges in rural areas, the number in urban areas is rising (ASCE 2009).

One of the main causes leading to degradation of reinforced concrete (RC) structures is the corrosion of steel reinforcement. Even though concrete acts as a physical barrier and steel passivity remains constant, once the alkalinity is reduced, depassivating anions can reach the steel reinforcement and trigger corrosion. The results may lead to spalling of the concrete cover due to the increase in the volume of steel from the formation of iron oxide. The corrosion of steel reinforcement is an electrochemical process, comprising both the reaction of oxidation, which involves the loss of electrons and the formation of metal ions, and reduction, which entails the gain of electrons in a chemical reaction (Figure 1).
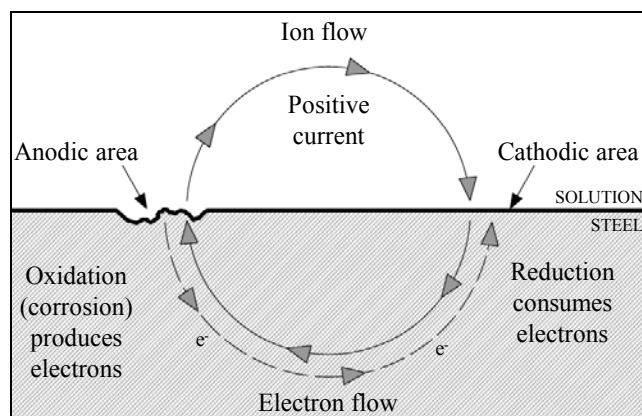
Figure 1 – Schematic of corrosion process of steel in saline solution

Four components must be present for corrosion to occur in a macro cell: the anode (where oxidation occurs), cathode (where reduction occurs), electrolyte solution, and metallic path. For the steel corrosion in concrete, the anode, cathode, and the metallic path are provided by the steel surface, while the electrolyte is provided by the moisture surrounding the steel.

The deterioration becomes especially detrimental for structures exposed to chlorides, such as seawater in coastal regions, and deicing salts in cold regions (Browne 1980; Hope et al. 1986; Allen et al. 1993). The corrosion process in marine environments can be modeled phenomenologically (Shalon and Raphael 1959, Melchers and Li 2006). Research shows (Ohtsu and Tomoda 2008) models of the deterioration due to corrosion that are typically divided into three phases (dormant, initiation, and accelerated), where the onset of corrosion is the discriminating point between the dormant and initiation phases, while the nucleation of cracks is the discriminating point between initiation and accelerated phases. In order to study durability, laboratory experiments are typically accelerated to provide usable results within a realistic period of time, recognizing that this procedure has its own disadvantages (Loreto et al. 2011).

The role of concrete cracks widths in relation to the onset and rate of corrosion of reinforcement is controversial. Research (Darwin et al. 1985) shows that corrosion is not clearly correlated with surface crack widths in the range normally found with reinforcement stresses at service load levels. Conversely, other studies (Otieno et al. 2010) conclude that the corrosion rate increases with crack width. For example, Andrade et al. (1993) report that no change in corrosion rate was recorded when a carbonated specimen was cracked; however, upon penetration of chlorides, the cracks do represent a

source of higher chemical aggression, because additional chlorides in a relatively high concentration can more effectively reach and depassivate the steel reinforcement.

The term acoustic emission (AE) is commonly used to describe both a technique and the physical phenomenon upon which the technique is based. The AE phenomenon consists of transient elastic waves that are generated by the rapid release of energy from localized sources within a material (ASTM 2010), while the AE technique uses one or more AE sensors to capture events that may take place in a bulk material. In order to acquire AE signals two different approaches exist. The first, referred to as hit driven (HDD), is threshold-controlled, with the AE wave data being acquired when the signal voltage exceeds a pre-defined threshold. Conversely, the second approach, referred to as time driven (TDD), is independent of any threshold setting. The AE wave, in fact, is recorded at a constant rate (i.e., every 5 s) for intervals of pre-determined length (i.e., each wave is 0.5 s). The fixed rate of acquisition makes TDD the best option when continuous AE phenomenon occurs. For both approaches, basic AE parameters can be evaluated and acquired upon collecting the AE waveforms. Among the HDD parameters, some of the most commonly used are amplitude, duration, and signal strength. The definitions, that are keys for the interpretation of the results of this study, are presented in Table 1, along with two TDD parameters, namely average signal level (ASL) and absolute energy (AbE).

Table 1 – Definition of basic AE features used in analysis

Amplitude	Peak voltage of the largest excursion attained by the signal waveform from an emission event. Amplitude is reported in dB_{AE}
Duration	Time from the first threshold crossing to the last threshold crossing of the linear voltage time signal
Signal Strength	Measured area of the rectified AE signal with units equal to pico-volt-sec
ASL	Time averaged AE logarithmic signal, measured on the AE amplitude logarithmic scale and reported in dB_{AE} units (where 0 dB_{AE} refers to 1 µV at the preamplifier input)
AbE	Energy contained in an acoustic emission signal, which is evaluated as the integral of the volt-squared function over time. AbE is reported in atto joules

AE is an effective technique for the detection of localized corrosion. The chemical and petrochemical industry, for example, has implemented this technology to detect stress corrosion cracking (Proust et al. 2001), pitting (Fregonese et al. 1999) and crevice corrosion (Kim et al. 2003) in stainless steel. Good results have also been achieved in the detection and localization of the initiation and progression of cracks originating from the corrosion of steel reinforcing bars in concrete (Li et al. 1998; Yoon et al. 2000; Idrissi and Liman 2003). In addition, it has been shown that AE can provide warnings of the early stage of corrosion, and that cumulative AE activity can be correlated with the severity of corrosion (Ohtsu and Tomoda 2008). In fact, research shows that when cumulative signal strength (CSS) is plotted versus time, the CSS will generally increase sharply at a certain time. This is typically referred to as the "knee" in the cumulative curve often correlated to damage (Ziehl et al. 2008) and corrosion (Ohtsu and Tomoda 2008). Finally, the use of standard piezo-electric AE sensors was demonstrated in the laboratory for the detection of the onset of the corrosion process in reinforcing bars (Ohtsu and Tomoda 2008), when no corrosion products were observed, while the

substantial vanishing of ferrous ions on the surface of steel bars was observed using a scanning electron microscope.

Research significance

The work presented in Study 1 is part of a long-term project that aims at deploying the AE technology into the practice of structural health monitoring (SHM) including detection of the onset of corrosion in small portions of repaired or rehabilitated RC structures (Godínez-Azcuaga et al. 2012). The overarching goal of the project is to develop an AE self-powered device capable of acquiring and delivering AE data using a wireless system remotely connected to a base location. Due to the stringent power constraints inherent in small self-powered devices, this study presents an alternative AE methodology to detect the onset of corrosion that is well suited to low power requirements. In addition, this work intends to clarify the controversial role of cracks in the onset of corrosion of steel reinforcement in the specific case of marine environment.

Specimen concept and design

Small-scale RC specimens were designed to define baseline AE datasets to characterize and discriminate the onset and growth of corrosion mechanisms under a controlled laboratory environment. The idea is to design specimens that are representative of typical areas in RC elements near the clear cover that protects longitudinal (flexural) reinforcement and stirrups, when present. The specimen conceptually reproduces the bottom of an RC beam or slab exposed to the penetration of chloride ions (Figure 2).
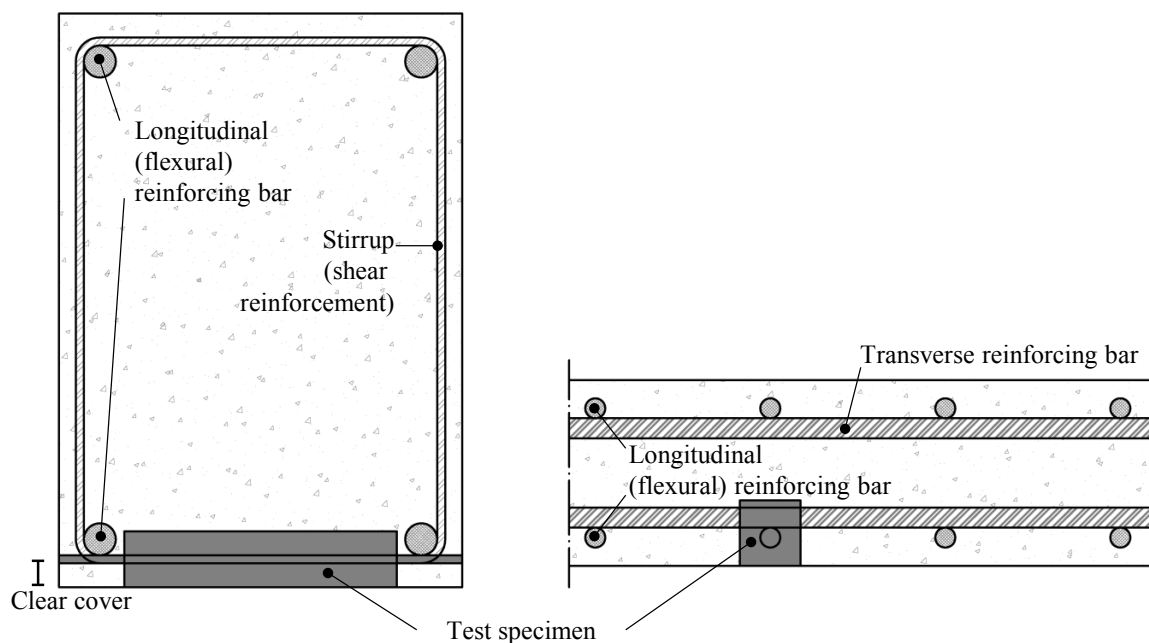
Figure 2 – Concept design of small-scale RC specimen (shaded area)

In order to investigate the coupling of (accelerated) corrosion and cracking, the specimen is notched (at casting) and later pre-cracked at the mid-length. The final design is an RC specimen with dimensions 90 mm × 90 mm × 510 mm and reinforced using a Ø13 mm (#4) steel bar with minimum specified yield strength of 410 MPa (Figure 3).
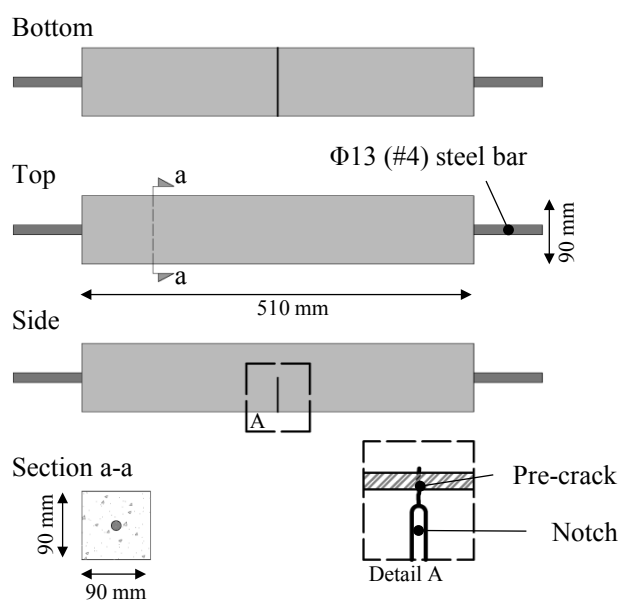
Figure 3 – Final design of small-scale RC specimen

Two different notch widths were used: hairline notch (0.2 mm), representative of a common condition in structurally sound bridge elements; and 0.8 mm wide notch, representative of a large crack width in a structurally deficient member (ACI 318 2011). The predefined notch widths at the mid-section were imposed using 20 mm deep metallic plates that were connected to the bottom of the molds during casting (Appendix 1). The specimens were then pre-cracked at the notched section, and past the steel bar, using a three-point bending setup.

The 28-day concrete compressive strength is determined by testing a total of three cylinders with 100 mm diameter according to ASTM C39. The results show a nominal strength of 54.1 MPa (with standard deviation of 0.2 MPa). By comparing the mixture design (Table 2) with different mixtures reported in the literature (Higgins 1995), a relatively low diffusivity coefficient is estimated ($D = 1.9 \times 10^{-12}$ m/s^2) that is typically associated with low-porosity concrete. This kind of concrete is commonly encountered, just as the cracks are, in structures that can be affected by corrosion despite the good quality of the material.

Table 2 – Concrete mixture design

			Aggregates				
f'$_c$ [MPa]	w/c [%]	a$_g$ [mm]	Gravel [kg/m^3]	Sand [kg/m^3]	Cement [kg/m^3]	Water [l/m^3]	Air Content [%]
54.1	0.47	4-12.5	860	540	400	188	3.0

Note:
f'$_c$ = nominal compressive strength; w/c = water cement ratio;
a$_g$= maximum aggregate size.

Test matrix

A typical test includes three specimens with same notch width subjected to accelerated corrosion at three different stages (Stage 1 – 1 day of exposure in a salt water solution; Stage 2 – 3 days of exposure; and Stage 3 – 5 days of exposure). At the same time, a fourth specimen with a stainless steel bar was exposed to the saline solution without being subjected to accelerated corrosion, in order to isolate the AE noise. For each of the two notch widths covered, the test was repeated three times. The test matrix is summarized in Table 3.

Table 3 – Test matrix

| Specimens | | | Test Duration | Repetitions |
Notch Width	Steel	Stages	Days of Accelerated	
0.2	M	1	1	3
	M	2	3	3
	M	3	5	3
	SS	3	Not Acc. Corr.	3
0.8	M	1	1	3
	M	2	3	3
	M	3	5	3
	SS	3	Not Acc. Corr.	3

Note:
M = Mild steel; SS = Stainless steel; Not Acc. Corr. = Not undergoing accelerated corrosion.

Accelerated corrosion test setup

In order to provide useful results within a realistic period of time, corrosion laboratory tests were accelerated by using an electrolytic cell. The electrolyte is a 3% NaCl solution, which is representative of marine environments (Ohtsu and Tomoda 2008; Ballim and Reid 2003); the reinforcing bar is used as the anode to undergo corrosion; and a copper plate is the cathodic element (Figure 4).
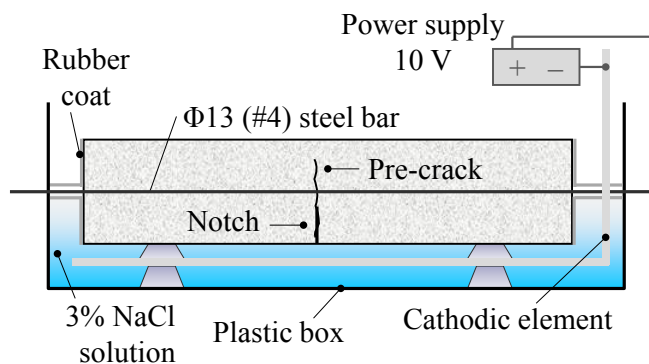
Figure 4 – Accelerated corrosion test setup, side view

The external driven voltage (10 V) is applied using a DC power supply. A plastic box was used as the container for the electrolytic cell setup since it is neutral to the redox reaction. To prevent corrosion of the protruding reinforcing steel portions, the exposed steel and the square concrete surfaces were wrapped with an elastomeric waterproof material. The specimens were placed in a protective structure that insulates them from the environmental noise. The protective structure was built using two boxes made of wood and soundproof foam, one placed inside the other, to take advantage of the soundproof effect of the air in between (Appendix 1).

Measurement setup

This research aims to identify the onset of the corrosion by means of AE in RC specimens. Since the concrete is a low frequency propagation material, and cognizant that AE signals produced during the corrosion process have a main spectrum band in a low-frequency range (20 – 80 kHz) (Yuyama and Nishida 2002), AE sensors (Physical Acoustic Corporation 2005) with resonant frequency of 55 kHz were used. Three AE transducers were mounted on the top face of each RC specimen (Figure 5), where the

number of sensors and layout aims at minimizing measurement errors in source location (Han et al. 2001).
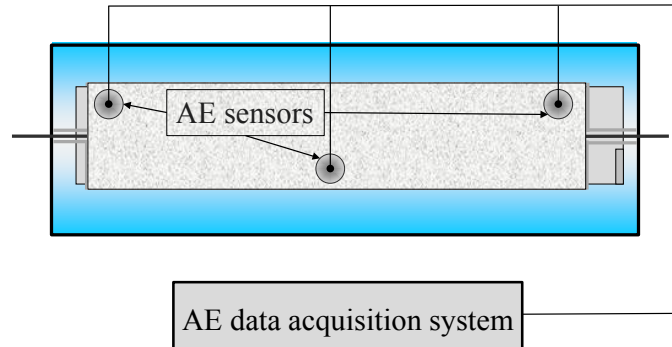
Figure 5 – AE test setup, top view

The data were acquired with a dedicated data acquisition system (Physical Acoustic Corporation 2009) that provides up to 16 AE channels and six analog inputs. Table 4 shows a summary of the typical parameters needed to reproduce the experiments performed in this study.

Table 4 – Summary of layout selected in AE data acquisition software

Parameter		Units	Value
Threshold		[dB$_{AE}$]	40
Analog Filter	Lower	[kHz]	1
	Upper	[kHz]	1000
Waveform Setup	Sample Rate	[MSPS]	5
	Pre-Trigger	[µs]	256
	Length	[points]	2024
Timing Parameters	PDT	[µs]	200
	HDT	[µs]	800
	HLT	[µs]	1000
	Max Duration	[ms]	1000

The AE threshold was set at 40 dB$_{AE}$ (ASTM 2010), assuming it is sensitive enough to detect the onset of corrosion (Ohtsu and Tomoda 2008), and, at the same time, allowing the acquisition of all the significant data. All the other parameters listed in Table 4 are not discussed herein, but their definition and value can be found in Physical Acoustic Corporation (2009). The HDD parameters recorded and stored include amplitude, duration, and signal strength. In addition, for each specimen (three sensors), TDD parameters are calculated at a constant rate (every 5 s) from an AE wave 0.5 s long. The recorded and stored TDD parameters are ASL and AbE. The former shows the least sensitivity because it is a logarithmic measure of the signal voltage; conversely, the latter has the highest sensitivity to changes in signal magnitude because it is proportional to the square of the signal voltage. The TDD parameters are filtered in the post-processing stage with a moving average, which is a type of filter that smooths data by replacing each data point with the average of the neighboring data points defined within a given time span.

Finally, the onset of corrosion is identified using cumulative AE parameters (Ohtsu and Tomoda 2008). A visual inspection method was selected among different strategies to choose the knee of the cumulative curve. This method, despite being dependent on the scale of the vertical axis, provides a straightforward way to analyze both HDD and TDD. Because the TDD curve is characterized by more gradual changes in slope attributed to smoothing out of the features over a longer time-span, typical knee detection methods are not as effective. Consequently, HDD knee-detection approaches, such as the use of the historic index (ASTM 2006, Ziehl and. Fowler 2003) cannot be used in its present formulation for knee determination on TDD data.

Benchmarks

In order to investigate the capability of AE to identify the onset of corrosion and characterize its progression, half-cell potential (HCP) measurement per ASTM C876 (2009) and linear polarization resistance (LPR) per ASTM G59 (2009) were implemented as well-established benchmark electrochemical techniques. The measurement of the corrosion potential of the reinforcement with respect to a copper-copper sulfate standard reference electrode (CSE), placed at the mid-section (above the pre-crack), was performed daily during the accelerated corrosion tests after disconnecting the power for a short period of time. A potentiostat (Gamry Instruments Inc. 2011) was used to carry out the LPR at the end of each Stage. The setup includes also a CSE as reference electrode and a Ti/MMO mesh as counter electrode. HCP values are known to provide only information on the probability of corrosion (ASTM 2009) while LPR results can be used to estimate the corrosion rate (ASTM 2004 – G102).

Results and discussion

Table 5 reports the electrochemical results at the end of Stage 1, including, for each specimen tested, the potential measured and the associated probability of corrosion. Table 5 also presents the AE results for the time of the onset of corrosion (in hours) estimated using CSS, ASL, and AbE as well as the acquisition rate (in points per second) for HDD and TDD data.

Table 5 – Results of HCP measurement and onset of corrosion estimation

Specimens		HCP [mV]	Corrosion Probability	CSS [h]	ASL [h]	AbE [h]	Hit Driven [pt/sec]	TDD [pt/sec]
Notch Width	Repetitions							
0.2 mm - #1	I	-514.5	severe	9.1	5.3	8.6	6.8	
	II	-521.3	severe	4.4	3.0	3.0	5.0	
	III	-491.9	high	5.4	5.2	5.2	11.0	
0.2 mm - #2	I	-437.8	high	15.8	11.3	15.3	0.4	
	II	-514.4	severe	7.4	7.0	7.1	4.3	0.6
	III	-540.4	severe	7.7	7.7	8.1	0.5	
0.2 mm - #3	I	-481.4	high	10.9	6.3	11.1	3.2	
	II	-481.4	high	2.2	4.3	4.3	0.6	
	III	-523.8	severe	4.0	3.6	4.1	3.1	
	Mean	-500.8	-	7.4	6.0	7.4	3.9	0.6
	St. Dev.	29.2	-	3.9	2.4	3.7	3.3	0.0
0.8 mm - #1	I	-501.7	severe	2.9	2.8	3.0	4.5	
	II	-462.4	high	8.5	4.4	4.4	1.1	
	III	-492.2	high	2.0	1.2	1.7	1.7	
0.8 mm - #2	I	-485.5	high	5.8	5.7	5.8	8.6	
	II	-522.6	severe	4.2	4.1	4.2	3.6	0.6
	III	-470.7	high	8.1	7.7	7.8	10.4	
0.8 mm - #3	I	-465.0	high	4.6	4.8	4.9	4.1	
	II	-383.8	high	11.2	9.3	9.1	0.4	
	III	-392.1	high	7.9	7.1	8.5	0.8	
	Mean	-464.0	-	6.1	5.2	5.5	3.9	0.6
	St. Dev.	44.4	-	2.8	2.4	2.4	3.3	0.0

In order to determine in which Stage the onset of corrosion occurs, the results of the HCP measurement are used. HCP shows that after the first day of conditioning the measured potential is always more negative than -350 mV CSE and, therefore, there is a probability greater than 90% that corrosion is occurring on the reinforcing steel. In addition, the corrosion rate calculated at the end of Stage 1 using the LPR ranged between a minimum of 0.034 mm/year to a maximum of 0.102 mm/year, confirming the presence of active corrosion.

Once that corrosion is active at the end of Stage 1, the onset can be identified using cumulative AE parameters. For the specimens with a 0.2 mm notch, the results for the CSS curve plotted over time show the knee (sharp change in slope associated with AE activity) on average about 7 hours after the start of the test. The plot of CSS during Stage 1 for a representative specimen (0.2 mm - #2 II, Table 5) is presented in Figure 6 (a), as well as the typical results for the duration of AE waves acquired during the same stage (results for all specimens are in Appendix 1). Both the CSS curve and the duration are obtained considering all the three sensors mounted on the specimen. Figure 6 (b) and (c) show typical result for the TDD (ASL and AbE respectively), which will be discussed later in this section.
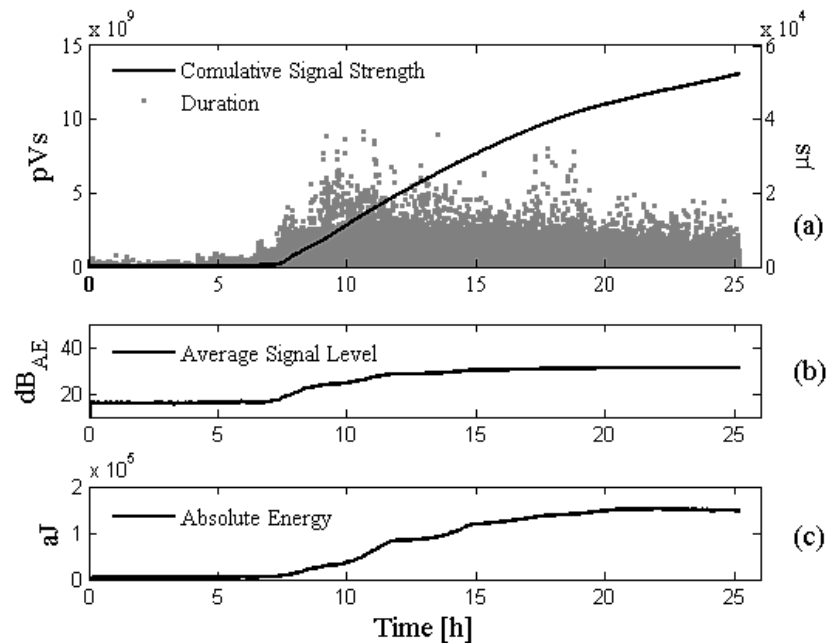
Figure 6 – Typical CSS and duration (a), ASL (b) and AbE (c) curves in Stage 1

The common approach to monitor corrosion with HDD parameters is based on the assumption that a burst release of energy is occurring. Figure 6 (a) shows that the AE waves acquired before the knee of the CSS curve are actually characterized by short

duration, which conversely greatly increases after the onset of corrosion. The extended duration can be explained by the increased energy of the AE signal as well as the presence of reflections (AE waves interfering with one another) due to the small geometry of the specimens. In addition, the longer duration suggests that corrosion may be studied as a continuous phenomenon and therefore TDD may be a good estimator for the onset of corrosion. Typical results for Stage 1 are presented in Figure 6, which includes the CSS curve (a) as a benchmark, the ASL (b) and the AbE (c). All the three curves show a sharp knee after about 7 hours.

Table 5 reports the onset of corrosion (in hours after the beginning of the test) identified with both CSS curve and TDD for all the specimens tested. The compatibility of TDD with the cumulative parameter results is investigated by studying their dispersion. For this purpose, a one-way ANOVA test (significance level, $\alpha = 5\%$, indicating the probability of a false rejection of the null hypothesis in the statistical test) was carried out under the null hypothesis that all the data are drawn from populations (CSS, ASL, and AbE) with the same mean, that is, the average of the estimated time of the onset of corrosion is the same for the three parameters considered. Table 6 and Table 7 show the results of this analysis considering separately specimens with notch width of 0.2 and 0.8 mm.

Table 6 – Results of ANOVA tests for specimens with notch width 0.2 mm

ANOVA
Estimated Time of Onset of Corrosion

	1) CSS - Notch Width 0.2 mm				
Populations:	2) ASL - Notch Width 0.2 mm				
	3) AbE - Notch Width 0.2 mm				

	SS	df	MS	F	p-value
Columns	12.81	2	6.40	0.49	0.62
Error	311.04	24	12.96		
Total	323.85	26			

Note:
SS = Sum of squares; df = Degrees of freedom; MS = Mean squares;
F = F-statistic

Table 7 – Results of ANOVA tests for specimens with notch width 0.8 mm

ANOVA
Estimated Time of Onset of Corrosion

	1) CSS - Notch Width 0.8 mm				
Populations:	2) ASL - Notch Width 0.8 mm				
	3) AbE - Notch Width 0.8 mm				

	SS	df	MS	F	p-value
Columns	3.87	2	1.94	0.27	0.77
Error	173.97	24	7.25		
Total	177.84	26			

Note:
SS = Sum of squares; df = Degrees of freedom; MS = Mean squares;
F = F-statistic

As per all the standard ANOVA tables, the columns represent respectively the sums of squares (SS), degrees of freedom (df), mean squares (MS = SS/df), F statistic, and p-value. The magnitude of the estimated p-value (0.62 for specimens with 0.2 mm notch, and 0.77 with a 0.8 mm notch) clearly indicates that there is not enough evidence to reject the null hypothesis. This suggests that TDD and cumulative parameter results may be considered compatible.

In addition, power consumption considerations are critical in the selection of the appropriate AE parameter to implement on a self-powered data acquisition system. A higher acquisition rate implies a more recurrent use of the analog to digital converter and therefore higher energy consumption. Table 5 reports the acquisition rate (in points per second) of each specimen for HDD and TDD data. The results show that on average the acquisition rate is higher for HDD data rather than TDD. This infers that a self-powered AE data acquisition system is more power efficient if it uses TDD data rather than HDD.

The results of Study 1 can also be used to discuss the controversial effect of notch width on the onset of corrosion in the specific case of exposure to marine environment. The mean time of the onset of corrosion estimated by the knee in the CSS curves is 7.4 hours for the case of hairline notch, and it decreases to 6.1 hours for the specimens having a notch width of 0.8 mm (Table 5). A similar trend can be recognized also when the onset of corrosion is estimated based on the ASL and AbE curves. An analysis of the variance was performed for the two different populations of data, the estimated time of onset of corrosion for specimens with notch of 0.2 mm and 0.8 mm. The null hypothesis is that all the data are drawn from populations with the same mean. The results are shown in Table 8.

Table 8 – Results of ANOVA test between specimens with
notch width 0.2 mm and 0.8 mm

ANOVA
Estimated Time of Onset of Corrosion

Populations:	1) Notch Width 0.2 mm 2) Notch Width 0.8 mm				
	SS	df	MS	F	p-value
Columns	23.60	1	23.60	2.45	0.12
Error	501.69	52	9.65		
Total	525.29	53			

Note:
SS = Sum of squares; df = Degrees of freedom; MS = Mean squares;
F = F-statistic

The minimum significance level that makes the null hypothesis being rejected is 0.12. Therefore, it can be concluded, only with a confidence interval (1-α) equal to 88%, that the two populations have a different mean. These results seem to be in line with the conclusion of Andrade et al. (1993): the wider the crack on the surface, the more chlorides penetrate from outside, which infers a more severe chemical aggression and, consequently, an earlier onset of corrosion.

Stages 2 and 3

After identifying the onset of corrosion during *Stage 1* with both cumulative parameters and TDD, the remaining stages can be investigated in terms of AE. Typical results (specimen *"0.2 mm - #2 III"*) at the end of *Stage 3* are presented in Figure 7, which includes CSS curve *(a)*, ASL *(b)* and AbE *(c)* plotted over the duration of the entire test (about 120 h), and considering all the three sensors mounted on the specimen.
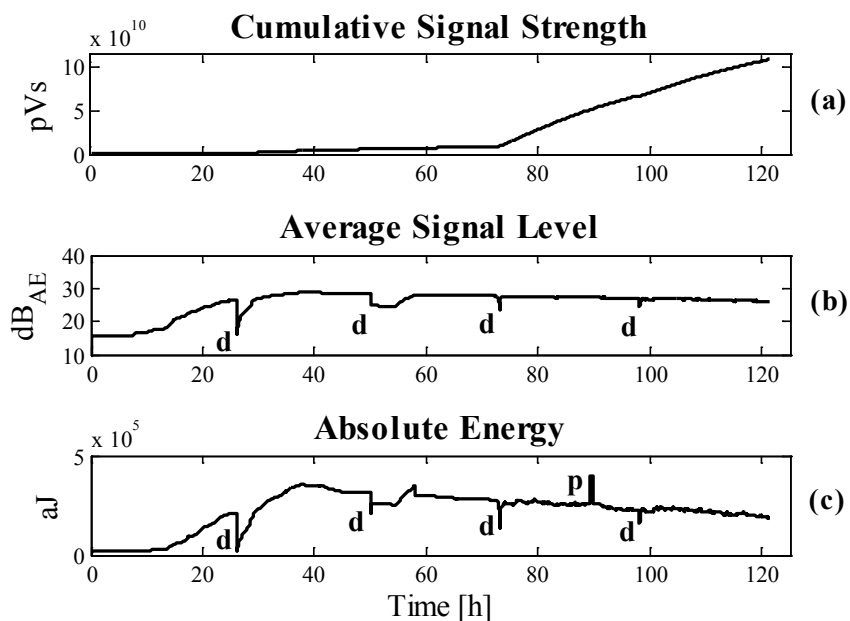
Figure 7 – Typical CSS (a), ASL (b) and AbE (c) curves in Stage 1, 2 and 3

It is noted that, since the scale in both axes of Figure 7 is different compared to Figure 6, the characteristic knee of the CSS curve during Stage 1 cannot be clearly identified in Figure 7. Nonetheless, the CSS curve presents a sharp increase during Stages 2-3 that can be associated with damage. In particular, recalling the phenomenological model proposed by Ohtsu and Tomoda (2008), this knee in the CSS curve may be associated with the nucleation of cracks in the concrete. This conclusion is supported by the behavior of the TDD. In fact, since the nucleation of cracks can be described as a burst release of energy, neither ASL nor AbE show a knee during Stages 2-3 and, conversely, their trend is nearly constant (Figure 7 (b) and (c)). In addition, the drops in both TDD curves (denoted by d in the Figure 7 (b) and (c)) coincide with the daily interruptions of the accelerated corrosion test to perform the electrochemical measurements, and are, therefore, irrelevant to the analysis. Also, since the high sensitivity of the AbE, the isolate peak, indicated as p in Figure 7 (c), can be explained with a temporarily increase of the AE activity but neither high nor long enough to be detected by the ASL curve. Finally, the conclusion,

according to which the knee of the CSS curve is associated with the nucleation of cracks, is verified in Figure 8.
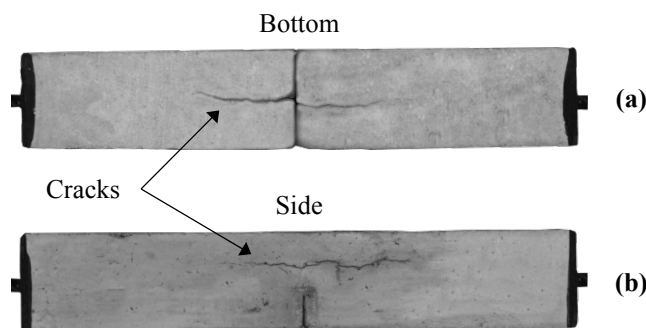
Figure 8 – Cracks at end of Stage 3

This picture, in fact, shows the presence of cracks at the end of Stage 3 in correspondence with the reinforcing bar on the bottom (Figure 8 (a)) and on the side (Figure 8 (b)) of specimen "0.2 mm - #2 III" (Table 5). Pictures of all specimens after the accelerated corrosion test are presented in Appendix 1.

Conclusions

In this study, an accelerated corrosion and AE monitoring test setup is presented. The effectiveness of AE in detecting the initiation of the corrosion phenomenon is discussed on the basis of results from small-scale pre-notched and cracked RC specimens. The salient outcomes are summarized as follows:

- The validity of the proposed setup is supported by the fact that the knee of the CSS curve is observed once a high (> 90%) probability of corrosion is inferred through standard half-cell potential measurement.

- The increased duration of the AE signals acquired after the onset of corrosion suggests that corrosion may be studied as a continuous phenomenon.

- Time driven ASL and absolute energy data show compatible results with those based on the CSS curves.

- Time driven data are better suited than hit driven data to low power conditions.

- Statistical analysis (88% confidence interval) seems to support the theory that in a marine environment, where chloride ions penetrate from outside the structure, a wider notch will lead to an earlier initiation of the corrosion process.

- After the onset of corrosion, CSS may be used to identify the nucleation of cracking, whereas TDD cannot be used for the same purpose due to the burst nature of the phenomenon.

This study demonstrates the suitability of AE technology for SHM by introducing a new TDD-based monitoring methodology to characterize the onset of corrosion. This alternative AE monitoring approach, coupled with well-established electrochemical techniques, is a promising tool to develop an early warning alarm system for corrosion in RC members.

CHAPTER 3: STUDY 2 - ACOUSTIC EMISSION FREQUENCY SPECTRUM OF REINFORCED CONCRETE UNDER ACCELERATED CORROSION

Summary

The advancement of structural health monitoring (SHM) techniques is intrinsically connected to the development of technology capable of acquiring, managing, integrating and interpreting structural performance data. One of the challenges in its application in the field of civil engineering is to deploy a more accurate and cost efficient technology capable of evaluating the deterioration of reinforced concrete (RC) structures for which the main cause of degradation is the corrosion of steel reinforcement. This process can be modeled phenomenologically, while laboratory tests aimed at studying durability are typically accelerated to provide usable results within a realistic period of time. Electrochemical measurements are well-established techniques for the monitoring of corrosion. However, since these techniques are typically intrusive, the demand for nondestructive techniques (NDT) has increased. Among the NDT methods recently studied, acoustic emission (AE) is emerging as a tool to detect the onset and progression of corrosion of metals. This study presents laboratory experiments where AE is employed to monitor small-scale RC specimens under accelerated corrosion. The frequency spectrum of the AE signals before and after the onset of corrosion is investigated in order to isolate the frequency components due to corrosion. Results show that the AE signal generated by the onset of corrosion excites only a narrow band of the frequency spectrum.

Background

One of the main causes leading to degradation of RC structure is the corrosion of the reinforcing steel. The deterioration becomes especially detrimental for structures exposed to chlorides, such as seawater in coastal regions, and deicing salts in cold regions (Browne 1980; Hope et al. 1986; Allen et al. 1993). Research shows (Ohtsu and Tomoda 2008) models of the deterioration due to corrosion that are typically divided into three phases (dormant, initiation, and accelerated). In these models the onset of corrosion, that physically is the breakage of the protective layer around the steel, represents the discriminating point between the dormant and initiation phases, while the nucleation of cracks is the discriminating point between initiation and accelerated phases.

One of the experimental difficulties, while studying durability, is to obtain usable results within a realistic period of time. Successful attempts to accelerate laboratory experiments include the addition of chlorides to the initial concrete mixture (Lee et al. 2000); the use of wet and dry cycles (Yuan et al. 2007); the increased capillarity suction (Nygaard and Geiker 2005), and the application of external potential (Idrissi and Limam 2003) or current (Ohtsu and Tomoda 2008).

In the first study, with an applied potential of 10 V, the onset of corrosion was detected, on average, as shortly as 8 hours from the beginning of test. Such a short initiation phase does not always allow for a comprehensive study of the features of the AE waves before the onset of corrosion. In addition, as a result of the applied voltage, the specimen is polarized, requiring quite a long time for depolarization, while voltage is disconnected, before the electrochemical test can be properly performed. In this study, in order to overcome these problems, the onset of the corrosion is accelerated by increasing the

capillarity suction. In particular this can be obtained by first subjecting the test specimens to a drying phase in a controlled climate after which they are exposed to a saline solution (Nygaard and Geiker 2005). Other factors that accelerate the ingress of chloride ions are a reduced cover thickness as well as concrete with a higher diffusivity coefficient (Loreto et al. 2011). However, the concentration of chlorides has little or no effect on the corrosion rate once corrosion starts (Melchers and Li 2006). Consequently, the increased capillarity suction can be used to obtain an earlier onset of corrosion but not to accelerate the corrosion process once started.

Finally, the onset of corrosion is identified locating the "knee" of the cumulative AE parameters curve over time (Ohtsu and Tomoda 2008). Historic index (H) has been found to be a sensitive method of detecting a change in slope in the CSS curve and is particularly valuable for determining onset of new damage mechanisms and is essentially independent of specimen size. The greater the number of hits on a channel, the more accurate the results. An analysis requires a minimum number of data points, and is not valid when less than 200 hits are recorded (Lovejoy 2008). The detection of significant AE in fiberglass reinforced plastic corresponds to an H equal to 1.4 (ASTM 2006, Ziehl and. Fowler 2003). However no value is available in the literature for its application on the onset of corrosion of RC structures.

Research significance

The work presented in this study is part of a long-term project that aims at deploying AE technology into the practice of structural health monitoring (SHM) including detection of the onset of corrosion in small portions of repaired or rehabilitated RC structures (Godínez-Azcuaga et al. 2012). This study presents an analysis of the frequency spectrum

of the AE signals in order to identify the main components excited before and after the onset of corrosion. A complete knowledge of the frequency domain not only allows filtering out unwanted signals during the acquisition, but also selecting AE sensors whose sensitivity is the highest in the frequency range of interest, thus improving the accuracy of the results.

Specimen design

Small-scale RC specimens were designed to define baseline AE datasets to characterize the onset of corrosion mechanisms under a controlled laboratory environment. The final design is an RC specimen with dimensions 90 mm × 150 mm × 610 mm. A single Ø13 mm (#4) reinforcing steel bar with minimum specified yield strength of 410 MPa is embedded with 40 mm cover thicknesses (Figure 9). The clear cover is locally reduced at the mid-section up to 20 mm by inserting a plastic tab during the casting (Appendix 2).
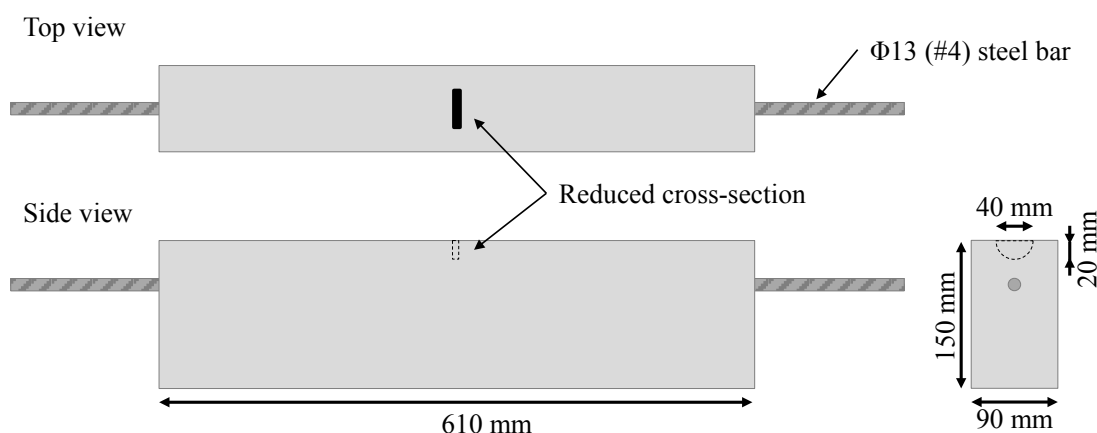

Figure 9 – Small-scale RC specimen

The 28-day concrete compressive strength is determined by testing a total of six cylinders with 100 mm diameter according to ASTM C39. The results show a nominal strength of 24.6 MPa (with standard deviation of 0.9 MPa). By comparing the mixture design (Table 9) with different mixtures reported in the literature (Higgins 1995), a relatively

high diffusivity coefficient is estimated ($D = 7.1 \times 10^{-12}$ m/s^2). The choice of this parameter is important because a high diffusivity allows a more rapid penetration of chlorides, and therefore an earlier onset of corrosion.

Table 9 – Concrete mixture design

f'$_c$ [MPa]	w/c [%]	a$_g$ [mm]	Gravel [kg/m^3]	Sand [kg/m^3]	Cement [kg/m^3]	Water [l/m^3]	Air Content [%]
			Aggregates				
24.6	0.48	12.5	470	1120	310	148	3.0

Note: f'$_c$ = nominal compressive strength; w/c = water cement ratio;
a$_g$= maximum aggregate size.

Accelerated corrosion test setup

In this study the corrosion process was accelerated without imposed current. The specimens were dried in an environment with controlled temperature and humidity (20 days at 20°C and 75% rh) after the initial curing of 28 days. Once the drying procedure was complete, the specimens were exposed to a saline solution typical of marine environments (3% NaCl) (Ballim and Reid 2003). A plastic box, placed on top of the specimen, was chosen as a container for the solution, because it is neutral to the red-ox reaction. The setup is presented in Figure 10. With this configuration, the solution enters the sample by gravity and the reduced moisture in the specimen generates capillarity suction that provides additional chloride ions transport. Finally, the cover thickness was locally reduced in order to expedite the chloride ingress.
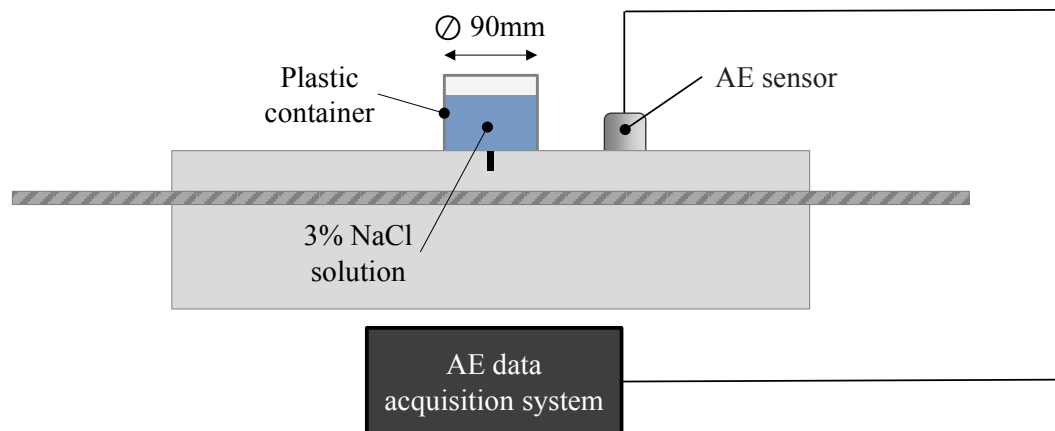
Figure 10 – Test setup, side view

Test matrix

The test includes four specimens subjected to accelerated corrosion for five days. At the same time, a fifth specimen with a stainless steel bar was exposed to the saline solution without being subjected to accelerated corrosion, in order to isolate the unwanted AE signals.

Measurement setup

The main objective is to characterize the AE spectrum at the onset of corrosion in RC specimens. Since the concrete is a low frequency propagation material, and cognizant that AE signals produced during the corrosion process have a main spectrum band in a low-frequency range (20 – 100 kHz) (Yuyama and Nishida 2002), AE differential sensors (Physical Acoustic Corporation 2011) with good sensitivity over the whole range of 35 - 100 kHz were used. One AE transducer was mounted on the top face of each RC specimen (Figure 10). The data were acquired with a dedicated data acquisition system (Physical Acoustic Corporation 2009) that provides up to 16 AE channels and six analog inputs. Table 10 shows a summary of the typical parameters needed to reproduce the experiments performed in this study.

Table 10 – Summary of layout selected in AE data acquisition software

Parameter		Units	Value
Threshold		[dB$_{AE}$]	30
Analog Filter	Lower	[kHz]	20
	Upper	[kHz]	100
Waveform Setup	Sample Rate	[MSPS]	1
	Pre-Trigger	[μs]	200
	Length	[points]	1024
Timing Parameters	PDT	[μs]	50
	HDT	[μs]	200
	HLT	[μs]	300
	Max Duration	[ms]	99

The AE threshold was set at 30 dB$_{AE}$ (ASTM 2010), as this value is considered to be sensitive enough to detect the onset of corrosion (Assouli et al. 2005), and, at the same time, allows the acquisition of all significant data. Critical parameters for the acquisition of hit driven AE data are the hit definition time (HDT) and the hit lockout time (HLT). HDT is the maximum time that a counter, which restarts counting from zero each time the threshold is passed, can reach before the system closes a hit (Figure 11).
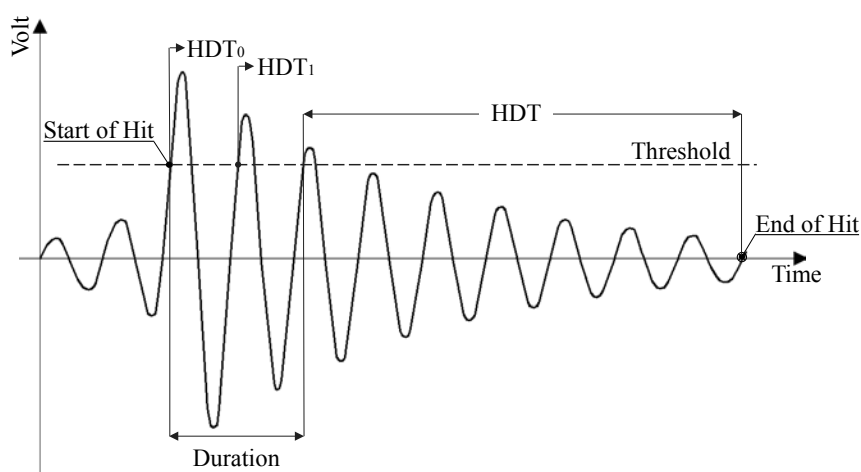

Figure 11 – Hit definition time and duration

HLT is the time after the end of the hit during which the system does not respond to any threshold crossing and is usually used to inhibit the measurement of reflections and late arriving signals. Because of the small dimension of the specimens, one of the sources of AE activity is the reflections that are caused by the boundaries of the specimen. In order to avoid an increase in the duration of the activity due to the reflections interfering with one another, HDT and HLT are selected respectively equal to 200 µs and 300 µs (Physical Acoustic Corporation 2009). All the other parameters listed in Table 10 are not discussed herein, but their definition and value can be found in Physical Acoustic Corporation (2009).

Finally, the specimens were placed in a protective structure that insulates them from the environmental noise. Such a structure was built using a box made of wood and soundproof foam (Appendix 2).

Electrochemical benchmarks

Well-established electrochemical techniques were carried out daily in order to monitor the different stages of the corrosion process. A potentiostat (Gamry Instruments Inc. 2011) was used to perform the half-cell potential (HCP), the linear polarization resistance (LPR), and, the electrochemical impedance spectroscopy (EIS) measurements. The setup includes also a copper-copper sulfate standard reference electrode (CSE) as reference electrode and a Ti/MMO mesh as counter electrode. HCP measurement, per ASTM C876 (2009), calculate the corrosion potential of the reinforcement and returns the probability of active corrosion, while LPR (ASTM G59 2009) and EIS (ASTM G106 2004) estimate the polarization resistance (R_p) and the solution resistance (R_s) respectively.

Finally, the corrosion current density (i_{cor}) is estimated as follow (ASTM G102 2004):

$$i_{cor} = 10^3 \cdot B / (R_p - R_s) \tag{1}$$

Where i_{cor} is in $\mu A/cm^2$ while R_p and R_s are in $\Omega \cdot cm^2$. The constant B is a characteristic of the polarization curves, and a value of 26 mV is commonly used for steel that is actively corroding in concrete (Andrade and Gonzalez 1978). The corrosion current density can be related with the speed of corrosion as proposed by Andrade et al. (2004) (Table 11). Levels of corrosion speed low, moderate and, high refer to an active state of corrosion.

Table 11 - Relationship between corrosion current density and corrosion speed

i_{cor} [$\mu A/cm^2$]	Corrosion speed
< 0.1	Negligible
0.1 – 0.5	Low
0.5 – 1.0	Moderate
> 1.0	High

Results and discussion

In order to determine the onset of corrosion, the outcomes of the electrochemical tests are used. The results for HCP, LPR and, EIS are presented in Appendix 2. In particular, when HCP measurements return high probability of corrosion B is selected equal to 26 mV. B, LPR and, EIS are then substituted in Equation 1 to calculate i_{cor} whose values for all specimens over the 5 days are summarized in Table 12.

Table 12 – Corrosion current density

Day	i_{cor} [$\mu A/cm^2$]			
	Specimen 1	Specimen 2	Specimen 3	Specimen 4
0	0.08	0.07	0.09	0.08
1	0.07	0.06	0.08	0.07
2	0.51	0.11	0.36	0.37
3	0.45	0.44	0.31	0.41
4	0.49	0.43	0.45	0.45
5	0.51	0.45	0.47	0.48

Note:
Results obtained considering a polarized area of 22.80 cm^2

Comparing these results for i_{cor} with Table 11, it is evident that the corrosion speed for all specimens at the end of the first day is negligible, while it increases to low or moderate corrosion speed at the end of the second day. Therefore, the accelerated test can be divided into three stages: dormant (first day), initiation (during the second day) and, active (days 3 to 5). Once corrosion is active in all the specimens, the test is interrupted because the increased capillarity suction cannot accelerate the corrosion process once started. AE data are analyzed for the different stages to identify the onset of corrosion and to study the frequency spectrum.

Day 1

AE activity is recorded in all the specimens during the first day of test. However, since no active corrosion is detected using electrochemical measurements, these AE acquisitions can be referred as unwanted signals and filtered. In this respect the AE activity can be divided into random and systematic "noise". The former is characterized by a flat frequency spectrum, that is, each frequency component has the same probability to be the peak. Systematic noise is that component of the noise that in consecutive repetitions remains constant. By applying this definition to the frequency spectrum, it implies that

peak frequency occurs at a preferential frequency component. Therefore, the probability for the preferential frequency to occur is higher than the others. The procedure to filter unwanted AE signals is based on the consideration that, for fixed frequency bandwidths, random noise has the same probability to occur while systematic noise probability changes. This procedure consists of:

- Calculate the Fourier transform of each acquired waveform and estimate the maximum peak of the frequency spectrum.

- Define the probability density function (pdf) of the acquired AE frequency peaks by counting their occurrences.

- Fit the pdf with a robust linear regression and calculate the 95% confidence intervals.

$$y = \beta_0 + \beta_1 x \tag{2}$$

- Create a statistical test to verify that the fitting equation is horizontal. The appropriate hypothesis are:

$$H_0: \beta_1 = 0$$
$$H_1: \beta_1 \neq 0 \tag{3}$$

- Remove the outliers (systematic unwanted signal).

The procedure is applied on the AE data acquired from the benchmark specimen and the results are presented in Figure 12.
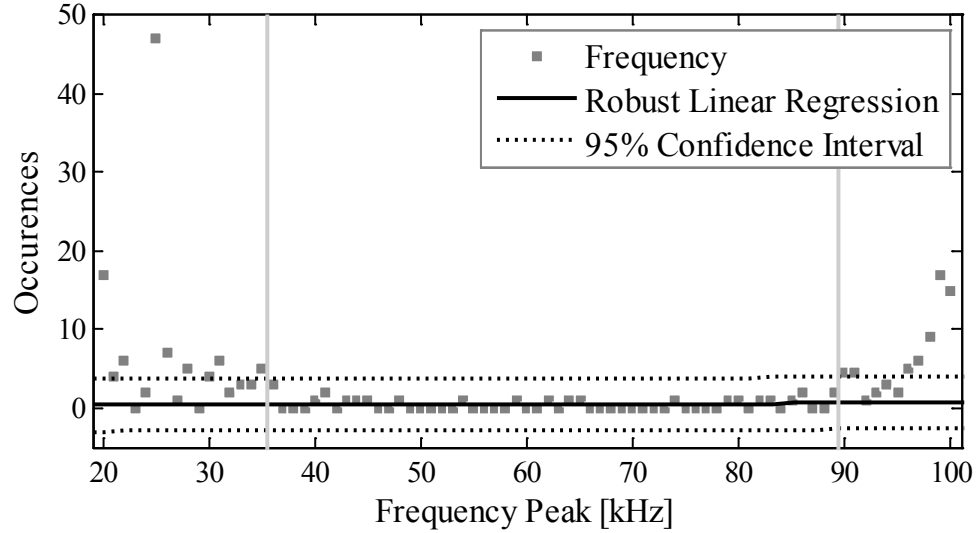
Figure 12 – Benchmark specimen, systematic unwanted signal filter

In this picture the grey squared symbols represent the occurrences of each frequency peak. This trend is the pdf multiplied by a constant factor equal to the total number of acquired hits. The black solid line is the calculated linear regression, while the dashed lines are the boundaries of the 95% confidence interval. Since the pdf is prone to outliers due to systematic noise, regular linear regression model returns unreliable computed statistics (confidence intervals). Thus, a robust fitting method is implemented given its lower sensitivity to large changes in small parts of the data. The estimated equation line, with R^2 equal to 0.929 is:

$$y = 0.3361 + 0.0035x \tag{4}$$

while the robust estimate for the standard deviation is equal to 0.987.

The statistic T_0 presented in Equation 5 can be calculated in order to test if the regression line is horizontal as described in details by Montgomery and Runger (2003).

$$t_0 = \beta_1/se(\beta_1) = 0.0035/0.0078 = 0.4487 \tag{5}$$

Where β_1 is the slope of the estimated regression line (Equation 2) and se(β_1) is the estimated standard error of the slope. In particular the statistic T_0 follows the t distribution with n-2 degrees of freedom. The null hypothesis is rejected if

$$|t_0| > t_{\alpha/2,n-2} \tag{6}$$

Since the reference value of t is $t_{0.0025,79} = 2.888$, the null hypothesis cannot be rejected. This implies that, by disregarding the outliers due to systematic noise, the pdf can be described with a horizontal line as expected if only random noise was recorded.

The main AE activity due to systematic noise is characterized by frequency peaks that are lower than 35 kHz and higher than 90 kHz. Since the specimen was isolated from environmental noise, this activity, both at low and high frequency, may be due to the infiltration of the saline solution into the pores of the concrete. However, in order to unambiguously identify the causes leading to the unwanted signals future tests will study the effect of geometry, material and sensor location. In this study, AE hits that are characterized by a peak frequency that is not in the range between 35 kHz to 90 kHz are considered systematic unwanted signal and removed from further analysis.

Once unwanted AE signals are filtered from the AE datasets, the frequency spectrum of all four specimens is studied during the dormant stage. For each frequency spectrum, the three highest peaks and their magnitude are calculated. Figure 13 shows the average magnitude of the peaks with at least three occurrences for the four specimens with steel bar.
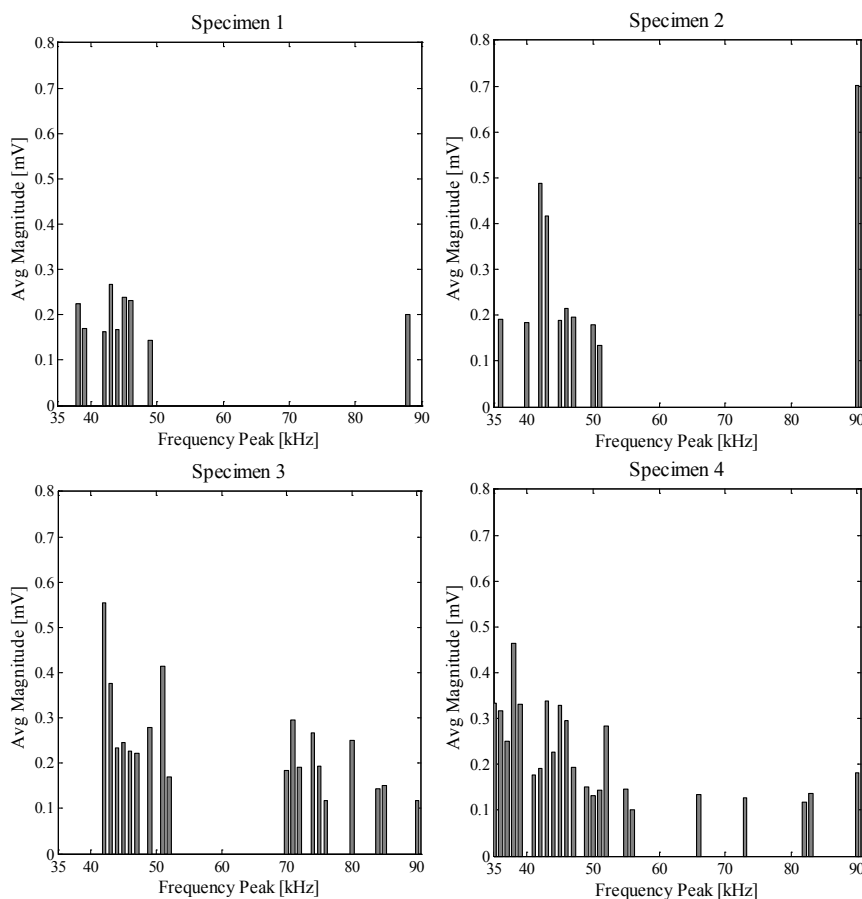
Figure 13 – Average frequency spectrum during dormant stage

Only specimen 3 acquires signals whose spectrum has relatively high magnitude peaks in the frequencies range between 70 kHz and 80 kHz. All specimens seem to have a frequency component close to 90 kHz probably part of the unwanted signals due to the infiltration of the saline solution. The only portion of the spectrum where all specimens consistently show magnitude higher than 0.2 mV is between 40 kHz and 50 kHz. This activity may be generated by the breakage of the protective layer around the reinforcing steel. This is in agreement with the electrochemical results that show active corrosion (protective layer already broken) only during the second day.

Onset of corrosion

After investigating the AE signal frequency distribution during the dormant stage, the historic index (H) is implemented to identify the "knee" in the cumulative signal strength (CSS) curve and therefore the onset of corrosion. This AE analysis considers data from the beginning of the test until the end of the second day, when the electrochemical measurements show active corrosion. The AE results for the CSS are consistent for all specimens and only specimen 4 is presented here (Figure 14) (the results for all the specimens are in Appendix 2). In particular, Figure 14(a) shows the CSS curve over time while H is plotted in Figure 14(b). Even if the knee of the CSS curve cannot be recognized with the selected scale of Figure 14(a), the H returns values greater than one. In particular, a peak of 1.2 is recorded and highlighted in both Figures 14(a) and 14(b) with a vertical dashed line. An enlarged view of Figure 14(a), indicated with A-A, verifies the presence of the knee in the CSS curve at the peak of the H. Comparable results are obtained for specimen 3 (peak of H equal to 1.9) while not enough hits are recorded for specimens 1 and 2 in order to calculate the H.
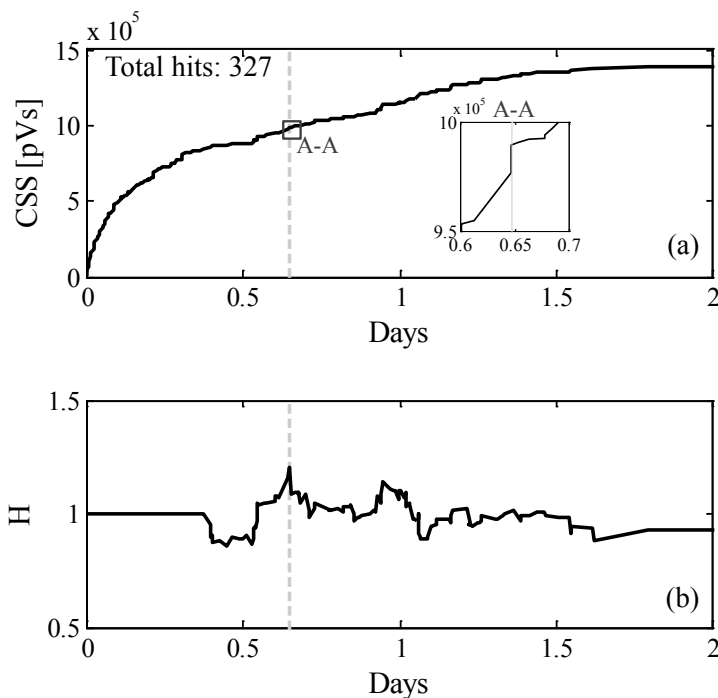
Figure 14 – Cumulative signal strength (CSS) and historic index (H)

The H seems to be an effective tool to identify the onset of corrosion during an accelerated test. In particular, the results suggest that, for the size of specimens and test conditions used, the detection of the onset of corrosion corresponds to H equal to 1.2. However, its application in the field may be limited because H can be calculated only when a minimum number of hits are acquired. In addition, the presence of noise may be an issue for the accurate estimation of H.

Day 3 to 5

Finally, the frequency spectrum after the onset of corrosion is studied in order to characterize the predominant frequency components of the corrosion during the initiation stage. For each frequency spectrum the three highest peaks and their magnitude are calculated. Figure 15 shows the average magnitude of the peaks with at least three occurrences.
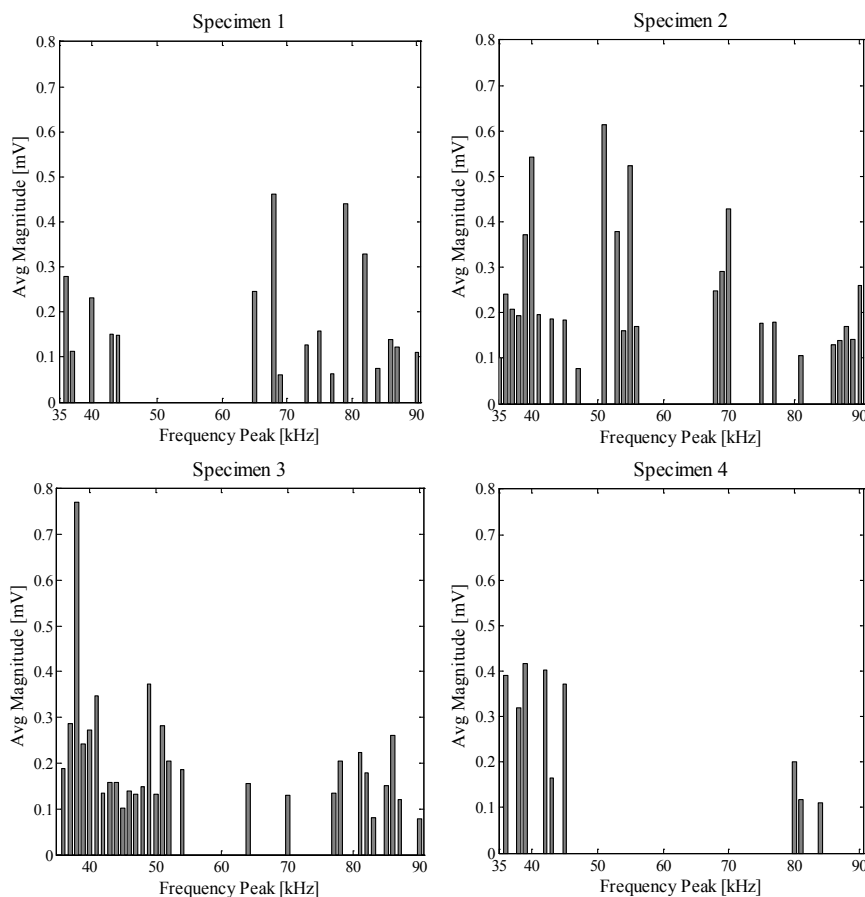
Figure 15 – Average frequency spectrum during active stage

AE activity is still present in the range between 40 kHz to 50 kHz suggesting that more protective layer is breaking along the steel bar. Compared to the initiation stage the activity increases for frequency higher than 65 kHz and lower than 40 kHz. The appearance of these new frequency components may be due to the active corrosion. However, since the new frequency components are different for each specimen, it is not possible to associate the phenomenon of active corrosion to a single frequency component.

Conclusions

In this study, an alternative accelerated corrosion and AE monitoring test setup is presented. Small-scale RC specimens are employed to study frequency spectrum of the

AE signal and the effectiveness of the AE technology in detecting the onset of corrosion. The salient outcomes are summarized as follows:

- The AE signals generated by the breakage of the protective layer around the reinforcing steel are isolated in the range of frequencies between 40 kHz and 50 kHz.

- The historic index seems to be an effective tool to identify the onset of corrosion during an accelerated test. In particular, the results suggest that, for the size of specimens and test conditions used, the detection of the onset of corrosion corresponds to H equal to 1.2.

- The validity of the proposed setup is supported by the fact that the knee of the CSS curve is observed before the corrosion becomes active.

- The historic index may find its implementation in the field limited because it can be calculated only when a minimum number of hits are acquired.

- AE signals generated by active corrosion excite several frequency components making it difficult to isolate them in a specific range.

This study demonstrates that the breakage of the protective layer of reinforcing steel, and thus the onset of corrosion, can be localized to a small portion of the AE frequency spectrum. This greatly improves the filtering of unwanted signals during the acquisition in the field. In addition, knowing the excitation frequency of the onset of corrosion allows the implementation of dedicated AE sensors whose sensitivity is the highest for the frequencies of interest, improving the accuracy of the results.

CHAPTER 4: STUDY 3 - ACOUSTIC EMISSION INTENSITY ANALYSIS FOR IN SITU EVALUATION OF REINFORCED CONCRETE SLAB

Summary

A three-story apartment building in the University of Miami campus built in 1947 and scheduled for demolition in the spring of 2011, was used as a research test bed. Two identical strips of the one-way reinforced concrete (RC) slab of the first floor of the building were saw-cut and load tested. In parallel with the well-established measurements of load and deflection, a continuous acoustic emission (AE) monitoring was carried out throughout the load test in order to estimate the AE evaluation parameters that relate to RC damage. The analysis of the AE results provides experimental evidence on the validity of AE technology as an assessment tool in the practice of in situ load testing.

Background

In the last decade, a different approach in the North American philosophy towards existing buildings has been observed. Rehabilitation and renovation of existing structures, as opposed to their demolition and reconstruction is taking hold of the public, owners, and practitioners. As a consequence, the practice of in situ load testing has become the object of renewed interest. In situ load testing is an important tool to assess the strength of existing buildings which is a prerequisite for their rehabilitation. However, the load test procedure currently adopted does not take full advantage of the progress in the measurement technology. By successfully implementing techniques such as acoustic emission (AE), there is an untapped potential to make the strength assessment of existing buildings more accurate and cost effective.

44

The work presented in Study 3 is part of a long-term project that aims at deploying the AE technology into the practice of structural health monitoring including in situ load testing (Godínez-Azcuaga et al. 2012). The building used as a research test bed is a three-story apartment building in the University of Miami campus that was constructed in 1947 and scheduled for demolition in the spring of 2011. This study describes the AE monitoring and evaluation of the in situ load test of two identical strips of the one-way reinforced concrete (RC) slab at the first floor of the building.

Research significance

Study 3 aims to develop an AE evaluation methodology based on the ACI 437 (2012) load test acceptance criteria in order to deploy AE technology as a monitoring tool for load tests. The overarching goal is to develop an AE monitoring system that enables to predict the ultimate capacity margin of an RC structure during a load test thus elevating what today is a "proof" test to a full-fledged prognostic event.

Background Research

AE Terminology

Since AE is a relatively young technology in structural health monitoring, its specific technical language is not yet sufficiently well-established in the civil engineering community. For this reason, some terms and parameters used in the remaining of this study are briefly defined in this section.

The general term AE, as per ASTM E1316 (2010), refers to the class of phenomena whereby transient elastic waves are generated by a rapid release of energy from localized

sources within a material, or to the transient waves so generated. Important features of the AE wave are amplitude and signal strength (Figure 16).
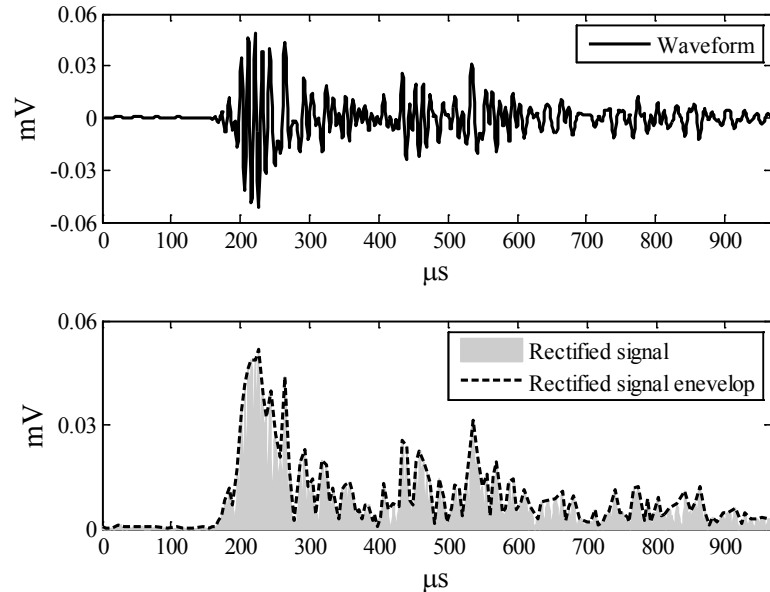

Figure 16 – AE waveform, amplitude and signal strength

The former is the peak voltage of the largest excursion attained by the waveform due to an emission event. The latter is the measured area under the rectified signal envelope with units proportional to volt-sec.

Fundamental concepts in AE evaluation are the Kaiser and Felicity effects which are, respectively, the absence or presence of detectable AE at a fixed sensitivity level, until previously applied stress levels are exceeded. Thus, the Felicity ratio can be defined as the ratio between the load at onset of significant AE activity during the current load cycle and the maximum previous load (Equation 7).

$$\text{Felicity ratio} = \frac{\text{load at onset of significant AE during reloading}}{\text{maximum load during previous loading history}} \tag{7}$$

The onset of significant emission is set as the first time the historic index (introduced below) during reloading exceeds a predetermined threshold chosen based on scale

geometry and material. In this study the threshold is selected equal to 1.15 (Liu 2007). The load corresponding to that time is the load at onset of significant AE.

Two AE evaluation parameters, both related to crack closure during unloading, are calm and relaxation ratios. The calm ratio is defined based on either cumulative AE activity (Ohtsu et al. 2002) (Equation 8) or cumulative AE energy (Liu and Ziehl 2009) which is estimated using the cumulative signal strength (CSS) (Equation 9):

$$\text{Calm ratio} = \frac{\text{cumulative AE activity during unloading}}{\text{cumulative AE activity during loading}}$$
(8)

$$\text{Calm ratio} = \frac{\text{CSS during unloading}}{\text{CSS during loading}}$$
(9)

The relaxation ratio differs from the calm ratio primarily in that the average signal strength is used in place of CSS (Colombo et al. 2005) (Equation 10):

$$\text{Relaxation Ratio} = \frac{\text{average energy during unloading}}{\text{average energy during loading}}$$
(10)

Another method to access structural performance using AE is the intensity analysis. Two factors are used in this analysis. One factor is the severity (S_r) and is defined as the average signal strength for the J hits having the largest numerical value of signal strength (Lovejoy 2008a) (Equation 11):

$$S_r = \frac{1}{J} \sum_{m=1}^{J} S_{Om}$$
(11)

In particular, J is an empirically derived value that depends on the material and, in this study, is set equal to 50. S_r does not apply until the number of acquired hits is greater than 50. S_{Om} is the signal strength of the mth hit, given that m is sorted in a descending

order based on the magnitude of the signal strength. The second parameter used in the intensity analysis is the historic index (H), which measures the change in signal strength throughout the test (Equation 12):

$$H(t) = \frac{N}{N-K} \frac{\sum_{i=K+1}^{N} S_{0i}}{\sum_{i=1}^{N} S_{0i}}; \quad \text{with} \quad K = \begin{cases} 0 & N < 200 \\ 0.8N & 200 \leq N < 1000 \\ N - 200 & N \geq 1000 \end{cases} \tag{12}$$

In Equation 12, N is the number of hits (sorted by time) up to time t while S_{0i} represents the signal strength of the ith hit. K is an empirically derived factor that varies with the number of hits, as shown in Equation 12. In order to determine the intensity of an AE source, H and S_r are calculated on data collected for each individual AE sensor during the loading phase and plotted on the intensity analysis chart. A typical example of this chart is presented in Figure 17 in which different regions are associated with different levels of damage (increasing from A to E).
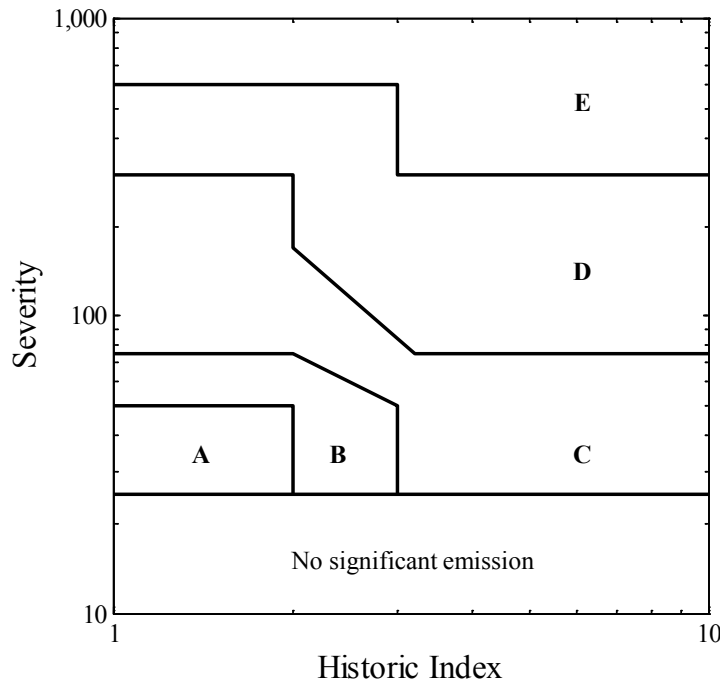

Figure 17 – Typical intensity analysis chart (Fowler et al. 1989)

AE evaluation of RC members

AE evaluation of RC members was first applied in the late seventies in Japan. Early studies (Ohtsu 1987) could prove not only that AE monitoring can discern different failure modes of RC beams (flexural-mode or shear-mode), but also that the Kaiser effect is observed in concrete. Later, independent researches (Hearn and Shield 1997 and Yuyama et al. 1999) stated that the Kaiser effect breaks down when a substantial damage is present in a RC member. Therefore, the Felicity ratio, already widely used to evaluate the structural integrity of fiber-reinforced polymer (FRP) vessels (ASTM E2478 2006), was introduced to quantify the Felicity effect. In particular, Felicity ratios equal to or above 1.0 indicate that the Kaiser effect is not violated, and vice versa. The Felicity ratio usually decreases when the maximum load increases (Hearn and Shield 1997); however, this correlation seems no longer to exist if a member experiences significant fatigue loads (Lovejoy 2008a), as nearly all in-service members in a civil structure.

A further indication of structural integrity is the level of AE activity during unloading. In fact, if a member is statically stable, AE activity is seldom observed in the unloading process (Yuyama et al. 1999, Ohtsu et al. 2002). To quantify this phenomenon, the calm ratio (Ohtsu et al. 2002) and the relaxation ratio (Colombo et al. 2005) are usually calculated. Both parameters generally do not change unless more damage is imparted to the RC member and, in particular, the ratios increase while the applied load increases (Lovejoy 2008b, Liu and Ziehl 2009). In addition, the calm ratio (if calculated using CSS) seems to decrease after the yielding of the reinforcing steel (Liu and Ziehl 2009).

The intensity analysis is a graphical method to assess structural performance using AE. The origin of this analysis is found in the structural evaluation of FRP structures (Fowler et al. 1989); however, more recent studies (Golaski et al. 2002, Lovejoy 2008a) showed its application also to RC and prestressed concrete (PC) members. The only attempted calibration of the intensity analysis chart with RC members is based on crack-mouth opening displacement of shear cracks (Lovejoy 2008a). Nonetheless, number and size of cracks in an RC member depend on how the RC member was designed and constructed. Therefore, while recognizing the importance of cracks as a possible indication of structural deficiency, it is not possible to quantify the damage based solely on the size of such cracks.

Experiment description

Geometry

The building was constructed in 1947, one of a series of look-alike three-story buildings and was occupied throughout the years as a dormitory. The structure consisted of a RC frame and infill masonry walls made of unreinforced concrete units. The floors at each level were one-way RC slabs. The thickness of the slabs at the first floor was 127 mm. Typical slab dimensions were 3.65 m wide in the north-south direction and 7.3 m long in the east-west direction (Figure 18).
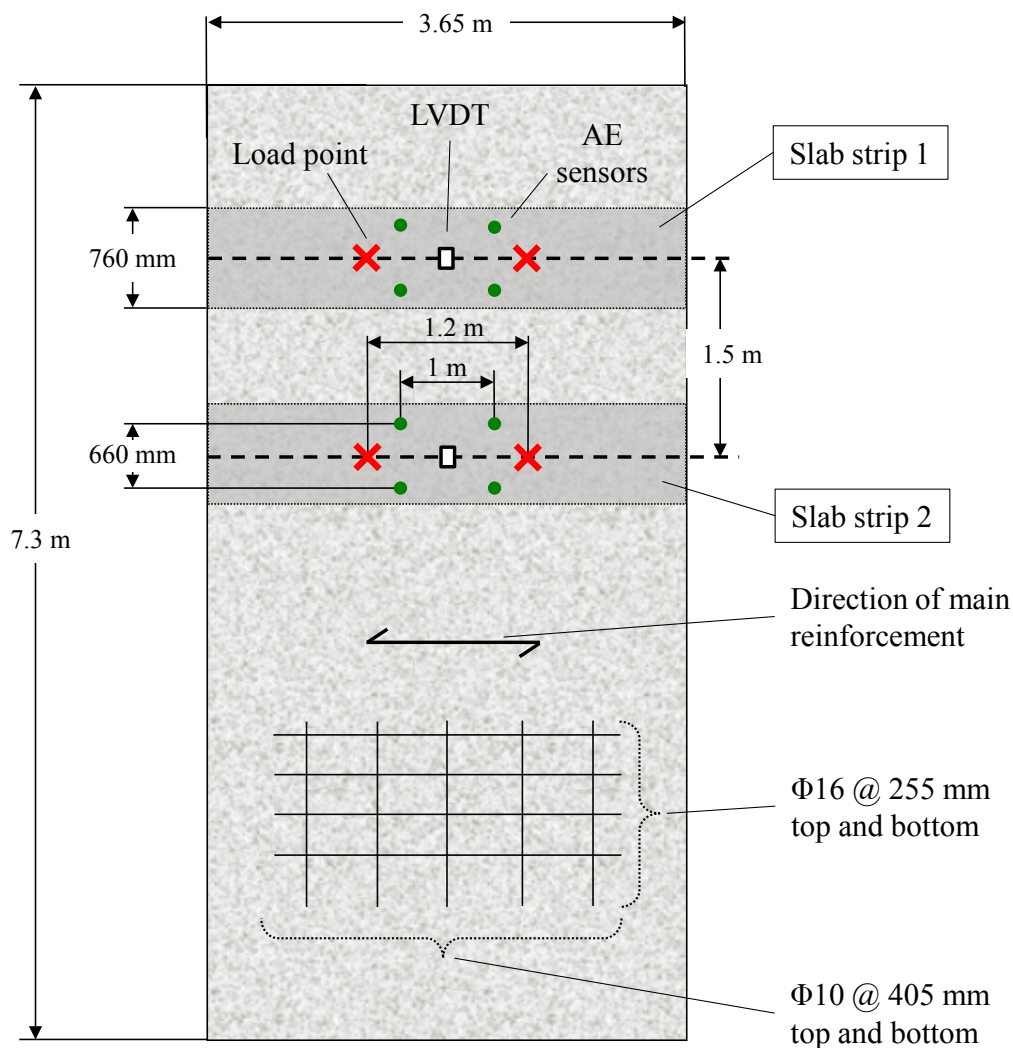
Figure 18 - Slab strip layout and measurement setup

The main reinforcement consisted of two layers of Φ16 bars spaced 255 mm center-to-center; while the transverse reinforcement consisted of Φ10 steel bars spaced 405 mm center-to-center. The concrete compressive strength was 20 MPa and the steel bars were smooth with yield strength of 448 MPa. To investigate the slab one-way behavior, two 760-mm wide strips were cut through one of the slabs of the building and load tested. The width of the strips was selected so that three reinforcing bars were included in the cross-section (De Luca et al. 2012).

Load test setup

As described in detail by De Luca et al. (2012), the load test was carried out using a push-down loading configuration (Figure 19).

Figure 19 – Load test setup

The load was applied by two hydraulic jacks of 445 kN capacity each, activated by a hydraulic hand pump. Each hydraulic jack was inserted between two steel spreader beams: the lower one was placed on top of a scaffolding along its short side (1.2 m); the upper one was in direct contact to the soffit of the slab of the second floor. As the hydraulic jacks extended, they pushed against lower and upper beams at the same time. The upper beams transferred the loads to the slab of the floor immediately above, which supplied the external reaction. 26.7 kN of sand bags were placed on the slab at the second

floor to prevent failure at the reaction slab. The lower beams transferred the load through the legs of a scaffolding tower to two points on the centerline of each slab strip. The two portions of the tower providing the load to the two strips were made independent during the test by removing the bracing. This ensured that each strip could move independently and receive load equally at two points. A square 150-mm in side steel plate was placed underneath each leg of the scaffolding tower to avoid localized damages as per ACI 437 (2012).

Loading procedure

A cyclic loading procedure is critical in the AE evaluation (Ridge and Ziehl 2006) since all the AE evaluation parameters are obtained as a relative measurement between cycles of the same magnitude. For this reason, the cyclic loading protocol described in ACI 437 (2012) is ideal for AE monitoring. This procedure consists of applying concentrated loads in a quasi-static manner to the structural member, in a total of at least seven cycles with each individual cycle including four to six load steps to be kept constant for 2 minutes. The first six cycles (Cycles A through F) are loading/unloading cycles. The paired cycles (loadsets) A-B, C-D and E- F are identical while the seventh cycle (Cycle G) was disregarded in the AE evaluation analysis since it does not include a repetition. To evaluate the structural results of the load test, ACI 437 (2012) defines three acceptance criteria: deviation from linearity (DfL), permanency index, and residual deflection. DfL was considered in Study 3 as a benchmark for the AE parameters.

The A-F load cycle procedure was repeated three times (Repetitions 1, 2 and 3). Repetition 1 is the load test as prescribed in ACI 437 (2012). If any of the three acceptance criteria is failed, ACI allows to repeat the load test (Repetition 2), as was the

case for this study. Repetition 3 was used here for research purposes and it is not part of the standard. In Repetitions 1 and 2, the maximum load applied at the fifth and sixth cycles (E-F) corresponds to the equivalent test load magnitude, TLM_{eq} (7.0 kN) (De Luca et al. 2012). TLM_{eq} produces a bending moment at the supports equivalent to the one produced by the factored uniformly distributed test loads magnitude as per ACI 437 (2012). In Repetition 3, the maximum load at cycles E-F was increased up to 20 kN such that cracks could generate at mid-span of the slab strips.

Load test instrumentation

The load was measured using two 110 kN load cells placed underneath the legs of the scaffolding, while the deflection at the mid-span of each slab strip was monitored using two linear variable differential transducers (LVDTs).

Four AE transducers were mounted on each slab strip (Figure 18). Since concrete is a low frequency propagation material and cognizant that for in situ monitoring of RC members the AE signals of interest have a main spectrum band in a low-frequency range between 20 kHz and 100 kHz (Ohtsu and Yuyama 2000), AE resonant sensors (Physical Acoustic Corporation 2005) with peak frequency of 55 kHz were used. The data were acquired continuously with a dedicated data acquisition system (Physical Acoustic Corporation 2009) that provides up to 16 AE channels. Table 13 shows a summary of the typical parameters needed to reproduce the test performed in Study 3.

Table 13 – Summary of layout selected in AE data acquisition software

Parameter		Units	Value
Threshold		[dB$_{AE}$]	55
Analog Filter	Lower	[kHz]	1
	Upper	[kHz]	1000
Waveform Setup	Sample Rate	[MSPS]	5
	Pre-Trigger	[µs]	256
	Length	[points]	2024
Timing Parameters	PDT	[µs]	400
	HDT	[µs]	600
	HLT	[µs]	800
	Max Duration	[ms]	1000

Even though a lower value is usually preferred to retain as much data as possible (Liu and Ziehl 2009), the AE threshold was set at 55 dB$_{AE}$ (ASTM E1316 2010) because of the presence of background noise. All the other parameters listed in Table 13 (i.e., analog filter, waveform setup parameters and timing parameters) are not discussed herein, but their definition and value can be found in Physical Acoustic Corporation (2009). The recorded hit driven parameters include amplitude, energy and signal strength. The parameters were then used to calculate the AE evaluation parameters necessary for the interpretation of the results.

Results and discussion

Load test results

The structural considerations that are used later in Study 3 to support the AE analysis are presented in this section. Focusing on the load test results, it was found that both slab

strips did not pass Repetition 1, making necessary Repetition 2. The load versus mid-span deflection plot for Repetitions 1 and 2 of slab Strip 1 is shown in Figure 20.
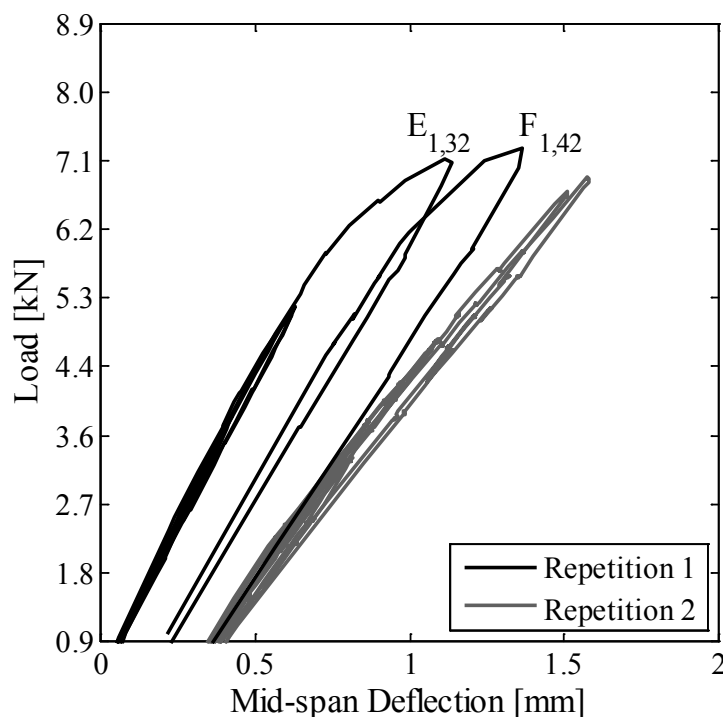

Figure 20 - Load vs. mid-span deflection for Repetitions 1 and 2 of slab strips 1

The cycles of Repetition 1 for which the DfL fails the acceptance criterion are labeled with a letter (i.e., the cycle) and two subscript numbers (the Repetition number and DfL value respectively). For example, $E_{1,32}$ means that during cycle E of Repetition 1 the DfL was 32%. In particular, the cycles identified by labels in Repetition 1 are E and F, while no cycles of Repetition 2 failed the acceptance criterion. The positive outcome of Repetition 2 entailed that the strip passed the load test. However, a further repetition was carried out with an increased load. Since the building had been selected for demolition, Repetition 3 was performed without concerns for damage. The load versus mid-span deflection plot for Repetition 3 of slab strip 1 is shown in Figure 21.
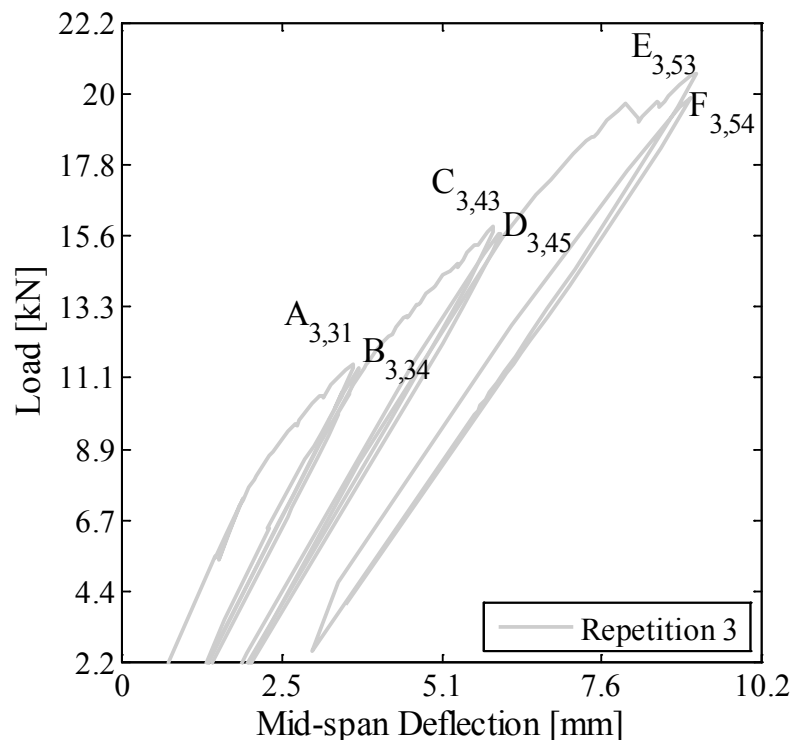
Figure 21 - Load vs. mid-span deflection for Repetition 3 of slab strips 1

DfL fails for all the cycles of Repetition 3, that are thus identified by a label equal to the one described above. Similar results were recorded for all the repetitions of slab Strip 2 with the only difference that in Repetition 1 the DfL criterion was never violated.

Additional results of the load test are presented by De Luca et al. (2012), including a discussion of the first six cycles (A to F) for slab Strip 2. This strip was more linear and experienced less permanent deflection than slab Strip 1.

AE results

Previous maximum experienced load

The onset of significant AE can be used to estimate the previous maximum load experienced by an RC member. This is obtained by considering the magnitude of the load

at the instant t when H exceeds 1.15 for the first time. This procedure is presented in Figure 22 for both slab strips.
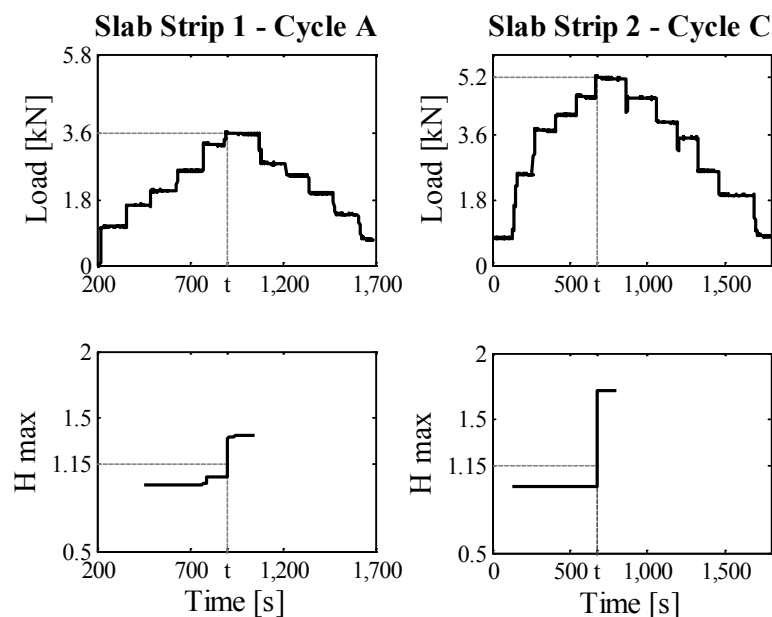
Figure 22 – Load and H max vs. time

The cycles during which significant AE activity is recorded for the first time are part of Repetition 1 and, in particular, they are cycle A for slab strip 1 and cycle C for slab strip 2. For each slab strip, the load and the maximum historic index value (H) are calculated by considering all the hits recorded by the four AE sensors connected to each slab strip, and are plotted over time. In addition, a dashed vertical line pinpoints the value of each curve at the time t, showing that the load is 3.6 kN for slab strip 1 and 5.2 kN for slab strip 2. This can be regarded as the load at each leg of the scaffolding tower equivalent to the previous maximum load experienced by each slab strip. This infers that slab strip 2 had seen higher loads during its life than slab strip 1. Therefore, AE analysis not only reaches the same qualitative conclusion presented by De Luca et al. (2012), but H exceeds 1.15 at the same time the maximum load is attained.

Hits threshold

In order for an AE analysis to be meaningful, a sufficient number of hits has to be recorded. This suggests that a threshold on the number of hits has to be introduced and for this study a tentative threshold of 200 hits is selected in both loading and unloading phases. This number is obtained as the product of the minimum number of hits per sensor (50) multiplied by the number of sensors (4) on each slab strip. The selected minimum number of hits per sensor is taken from the literature where the only AE parameter whose definition uses a threshold on the hits is the S_r that is calculated only when at least 50 hits are recorded by one sensor. The total number of hits acquired for each phase is summarized in Table 14.

Table 14 – Number of AE hits recorded for each strip throughout the test

Repetition	Max Load [kN]	Strip	Phase	Cycles					
				A	B	C	D	E	F
1	7	1	Loading	389	201	713	150	1118	1169
			Unloading	1	39	120	77	434	108
		2	Loading	89	120	279	46	1488	721
			Unloading	2	5	52	141	405	56
2	7	1	Loading	9	38	25	3	154	94
			Unloading	5	7	2	10	13	15
		2	Loading	10	29	43	7	100	83
			Unloading	8	2	2	7	23	11
3	20	1	Loading	6173	787	7031	1201	9852	1472
			Unloading	986	459	80	52	992	760
		2	Loading	6029	734	7695	1339	10269	1865
			Unloading	680	368	271	36	1168	3277

This table is structured so that each number of hits can be associated with the corresponding Repetition, maximum applied load, slab Strip and Cycle. In particular, the highlighted values represent those phases where the 200-hits threshold was exceeded. As the applied load increases, more cracks form and open and, therefore, more AE activity is

recorded. In particular, the number of hits acquired in Repetition 1 (7 kN) is an order of magnitude lower than in Repetition 3 (20 kN). The unloading phase of Repetition 1 features a scant number of hits, compared to the loading phase. This appears to indicate that slab strips are still in their elastic region. In fact, once permanent deflection is first observed in cycle E, the number of hits is also large in the unloading phase. In Repetition 2, since the level of load never exceeded the maximum one previously applied, a very limited amount of hits was acquired, confirming the sensitivity of AE activity to load history. Considering the scant number of acquired data and that the acceptance criterion (DfL) never failed, Repetition 2 was not taken into account for further analysis.

Intensity analysis chart

The use of AE as an assessment tool in load testing is conditional upon the obtaining of results compatible with the acceptance criteria prescribed in ACI 437 (2012). Thus, an attempt to calibrate the intensity analysis using one of these criteria (i.e., DfL) is presented. The intensity analysis charts for Repetitions 1 and 3 are shown in Figure 23, where severity (S_r) is plotted on the y-axis (logarithmic scale) while H is on the x-axis (linear scale).
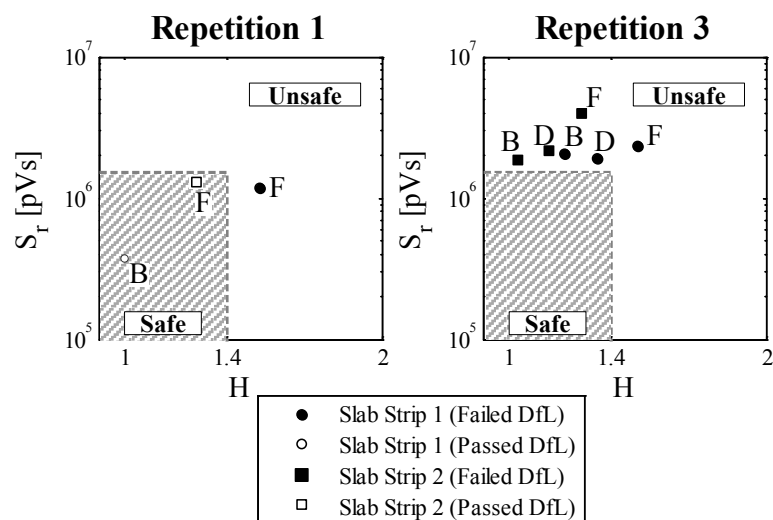
Figure 23 – Intensity analysis charts for Repetition 1 and 3 (both slab strips).
Acceptance criterion: deviation from linearity (DfL)

Each point (circles for slab strip 1 and squares for slab strip 2) is obtained as the average of the values of S_r and H calculated for the four sensors on each slab strip. In particular, in order to disregard those hits generated by an increased maximum load, only the second cycles of each loadset (B, D and F) are considered. In addition, among these cycles, only those in which the hits threshold was passed are investigated. The results from the DfL were also implemented in Figure 23 by representing the cycles that failed this criterion with solid symbols and that satisfied it with hollow symbols. The calibration was performed by graphically separating the solid symbols from the hollow ones. The results suggest that a univocal area represented by a shaded region in the intensity analysis charts can be marked off to clearly discern where the DfL acceptance criterion is satisfied. The proposed boundaries for such region are S_r equal to $1.5 \cdot 10^6$ pVs and H equal to 1.4. These graphs reveal the possibility of using AE to define a graphical acceptance criterion similar to the traditional material failure criteria (Budynas 1998). The analogy resides in the intuitive intelligibility offered by the chart where failure and acceptance points can be easily identified.

A further consideration on the intensity analysis is based on the nature of AE. Since this is a measure of a rapid release of energy (i.e., crack) in the form of transient elastic waves, the intensity chart is consequently the representation of a quantity independent from those (i.e., load and deflection) that are currently employed in ACI 437 (2012). This might offer the possibility to use the intensity chart to calibrate the threshold levels proposed by ACI 437 (2012) for the three acceptance criteria. To clarify this concept a graphical example is shown in Figure 24.
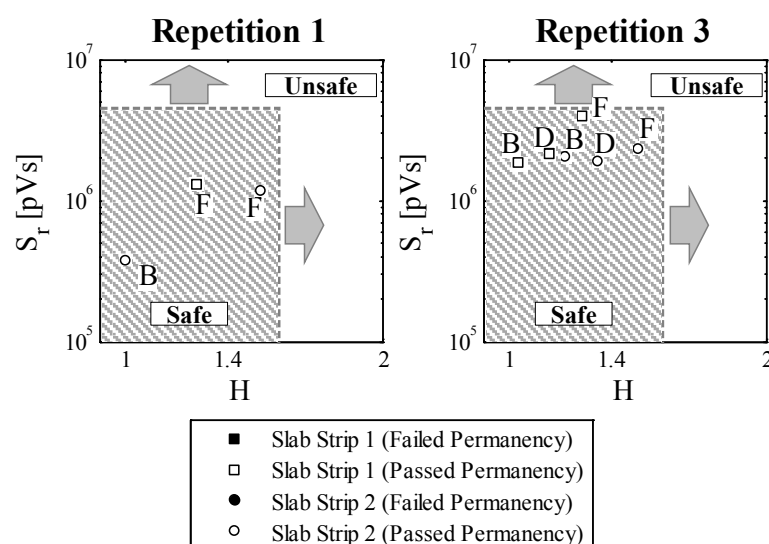
Figure 24 – Intensity analysis charts for Repetition 1 and 3 (both slab strips).
Acceptance criterion: permanency

In this plot, the intensity charts for Repetition 1 and 3, already presented in Figure 23, are re-proposed. The only difference is that the solid (failed criterion) or hollow (satisfied criterion) symbols are based on the results of the permanency acceptance criterion (ACI 437 2012) rather than DfL. Since permanency never failed, all symbols are hollow and have to be included in the acceptance shaded area. The arrows in the chart indicate the directions toward which the area could be expanded since it is not possible to define the upper limit of the acceptance area given the absence of solid symbols. More significantly,

the shaded area found when considering permanency (Figure 24) differs from the one obtained using DfL (Figure 23). From this, it may be inferred that the acceptance criteria proposed by ACI 437 (2012) may have to be re-tuned.

Conclusions

In Study 3, two identical strips of the one-way RC slab of the first floor of a building were saw-cut and load tested according to the new ACI 437 (2012) load test protocol. In parallel to the well-established measurements of load and deflection, an AE monitoring system was implemented. The outcomes of the AE monitoring and evaluation are summarized as follows:

- The onset of significant AE activity was used to estimate the maximum previous load experienced by an RC member. AE analysis not only reaches the same qualitative conclusion achievable by observing the load deflection curve, but it also estimates the value of the load possibly experienced by the member: 3.6 kN for slab strip 1 and 5.2 kN for slab strip 2.

- An insufficient number of recorded AE hits may lead to the calculation of scattered AE evaluation parameters. A threshold on the number of hits must be selected: 50 hits per sensor as proposed in the literature appear reasonable one.

- The intensity analysis chart was successfully calibrated based on the results of the deviation from linearity acceptance criterion established by ACI 437 (2012).

- The intensity analysis chart shows the potential to be used as a graphical acceptance criterion. The proposed acceptance region is within severity equal to $1.5 \cdot 10^6$ pVs and historic index equal to 1.4.

This study demonstrates the suitability of AE technology in the practice of in situ load testing. Even though more research is required to statistically corroborate the outcomes of this project, AE monitoring and in particular the intensity analysis chart seem to have an untapped potential to make the strength assessment of existing RC members more accurate and cost efficient.

CHAPTER 5: CONCLUSIONS AND RECOMMENDATIONS

This dissertation is articulated in three studies. The first two studies presented laboratory experiments where AE was employed to monitor small-scale RC specimens under accelerated corrosion. Study 1 investigated the effectiveness of an alternative AE monitoring approach to detect the onset of corrosion that is well suited to the low power requirements typical of long-term detection in the field. In Study 2, the frequency spectrum of the AE signals before and after onset of corrosion was analyzed in order to isolate the frequency components due to corrosion. In Study 3, two identical strips of the one-way RC slab of a building, scheduled for demolition, were saw-cut and load tested while AE monitoring was implemented, in parallel to well-established measurements of load and deflection, in order to define alternative acceptance criteria for damage assessment. The experimental and analytical evidence gained through these studies is herein summarized:

- The novel application of AE time driven parameters to monitor the onset of corrosion is well suited to low power conditions typical of long-term SHM.
- The AE activity of the breakage of the protective layer of reinforcing steel in concrete can be acquired and, in particular, its frequency components can be located in a small portion of the frequency spectrum.
- The AE intensity analysis chart has the potential to be used as a graphical acceptance criterion for damage assessment during the load test of RC members.

The results of this research add a new dimension to the existing AE methodology when used to identify and evaluate damage in RC members. AE detection of corrosion based on time driven parameters, coupled with well-established electrochemical techniques, is a promising tool to develop an early warning alarm system for structural health monitoring. In addition, knowing the frequency components of the onset of corrosion greatly improves the accuracy of the assessment. It was demonstrated that the AE sensors, whose sensitivity is the highest for the frequencies of interest, can be integrated in the monitoring setup with critical information pertaining to the definition of data mining-based filters in order to remove unwanted signals during the acquisition. Finally, if additional experimental evidence can corroborate the outcomes of Study 3, AE monitoring will offer a real-time graphical alternative acceptance criterion for the assessment of RC members' damage during load test.

The outcomes of this research are critical in the development of AE technology, however further research is needed in critical areas. Recommendations for future work include:

- Definition of data mining-based filters in order to remove unwanted signals during the acquisition. The effect of geometry, material and sensor location on the AE signal should be investigated for different stages of corrosion.
- Application of time-frequency analysis (i.e. Gabor transform and wavelet analysis) to study the transient nature of AE waves.
- Development of a real-time graphical acceptance criterion for the assessment of RC members' damage during load test based on the intensity chart

- Study the effectiveness of AE in predicting the remaining capacity of an RC structure. The sensitivity to scaling, geometry, material properties, degradation state, and AE sensor layout should be investigated.

APPENDIX 1: STUDY 1
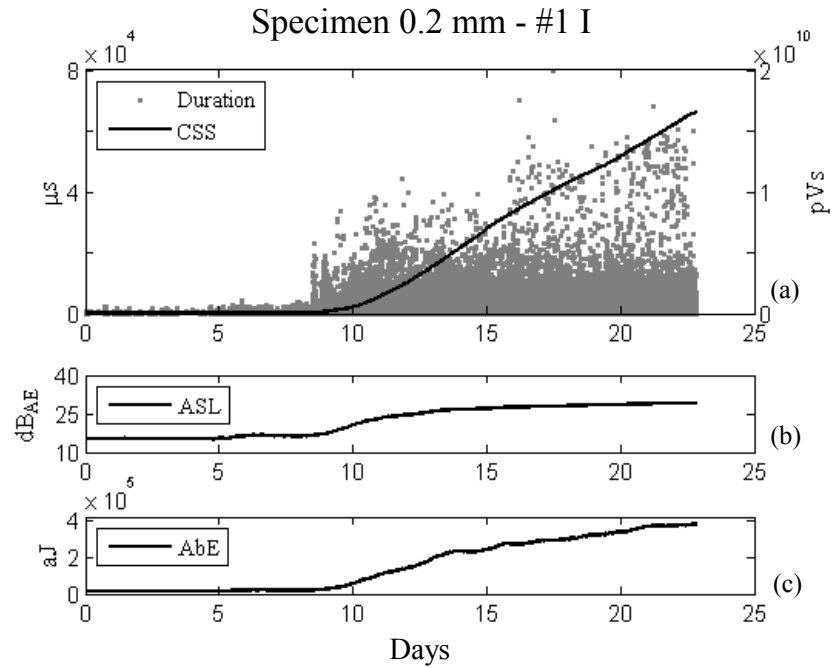
Specimen 0.2 mm - #1 I

Figure A.1 – Cumulative signal strength (CSS) and duration (a), ASL (b) and AbE (c)
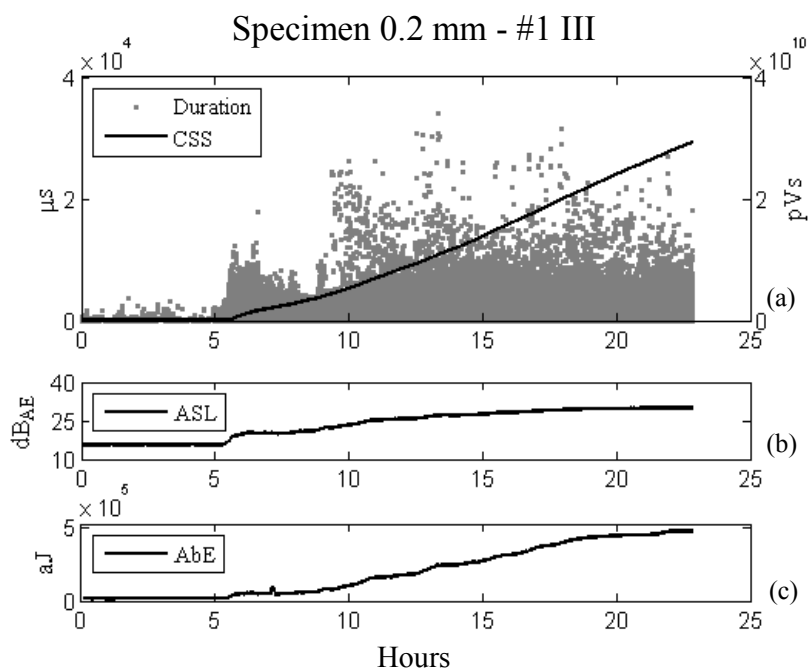
curves in Stage 1 for specimen 0.2 mm - #1 I
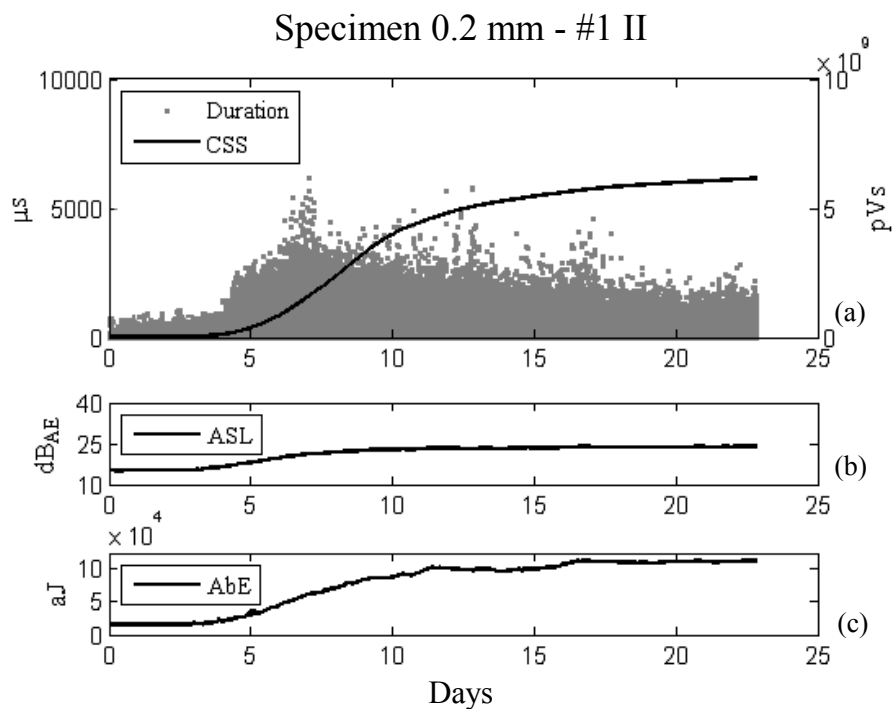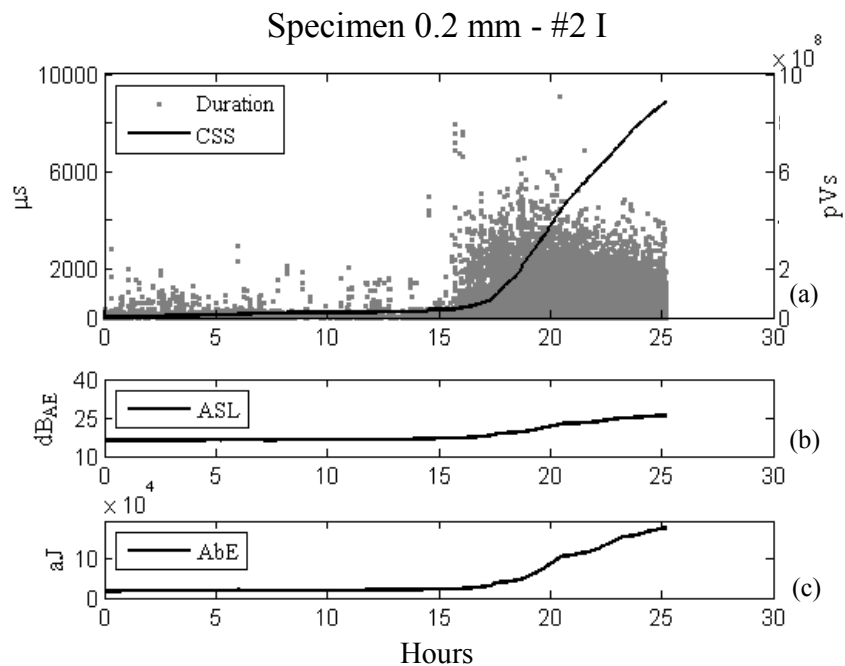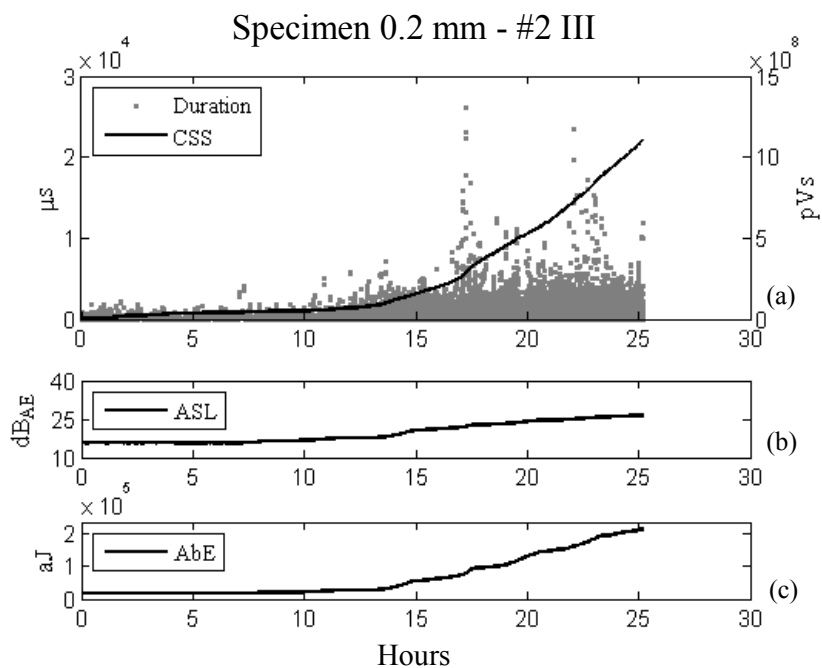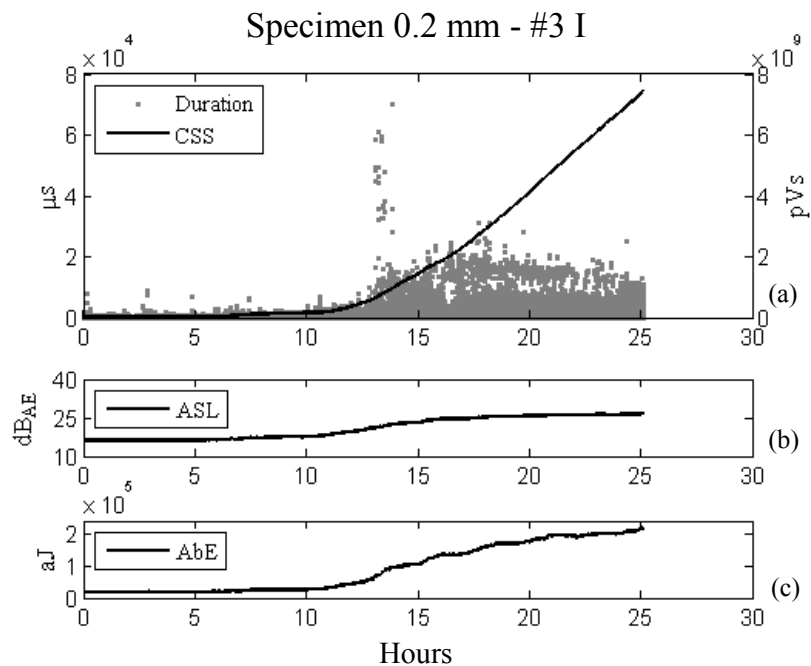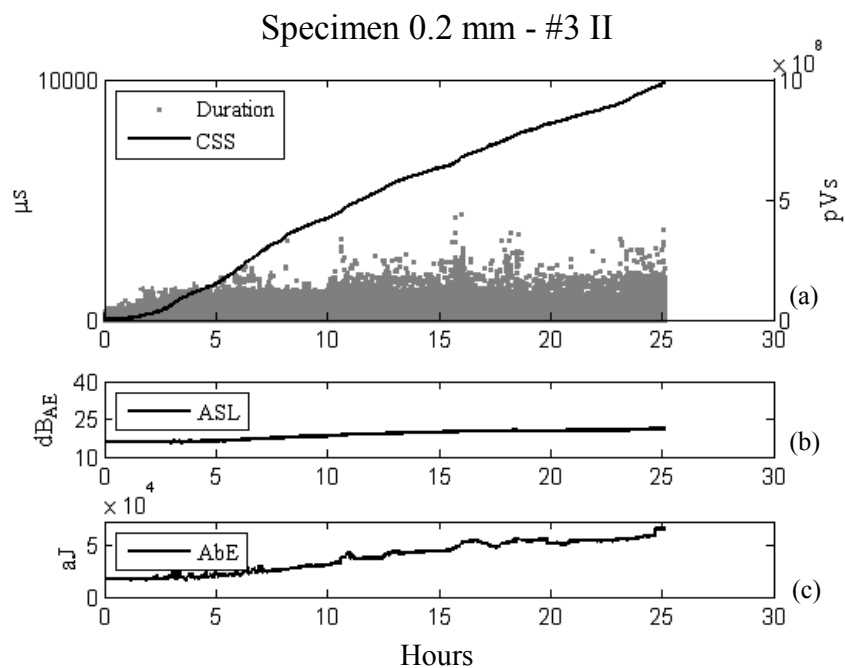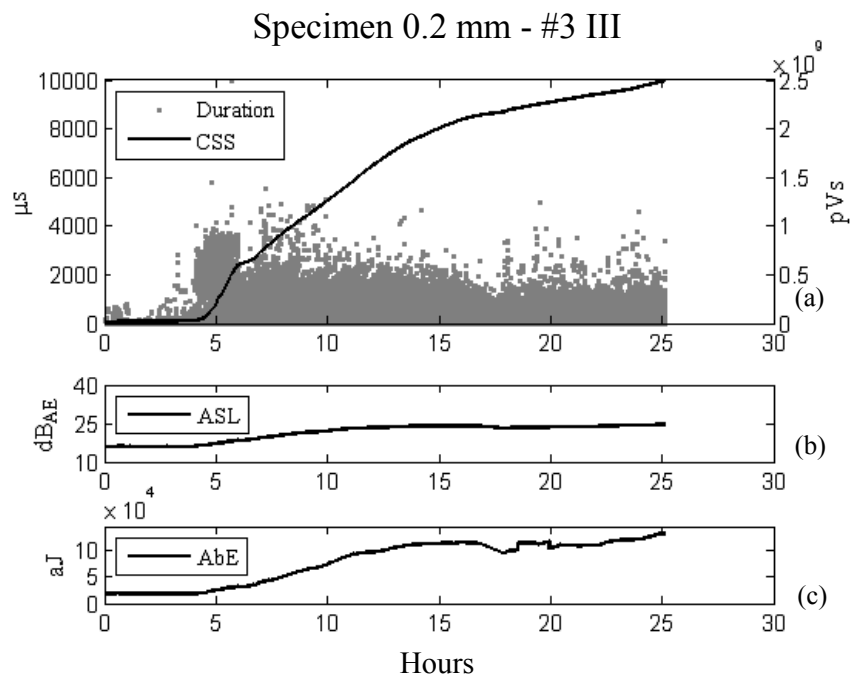
Specimen 0.2 mm - #1 II

Figure A.2 – Cumulative signal strength (CSS) and duration (a), ASL (b) and AbE (c)
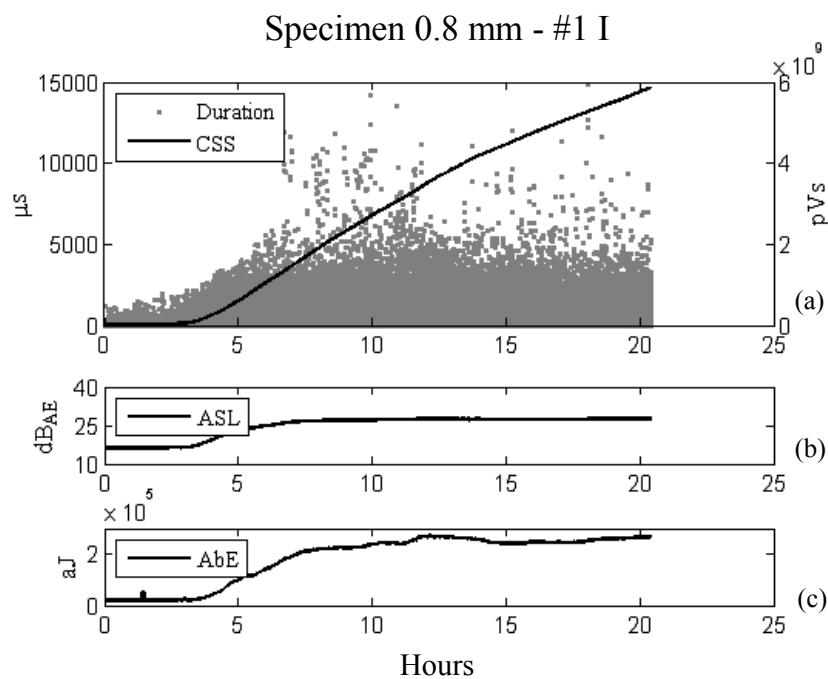
curves in Stage 1 for specimen 0.2 mm - #1 II

Specimen 0.2 mm - #1 III

Figure A.3 – Cumulative signal strength (CSS) and duration (a), ASL (b) and AbE (c)
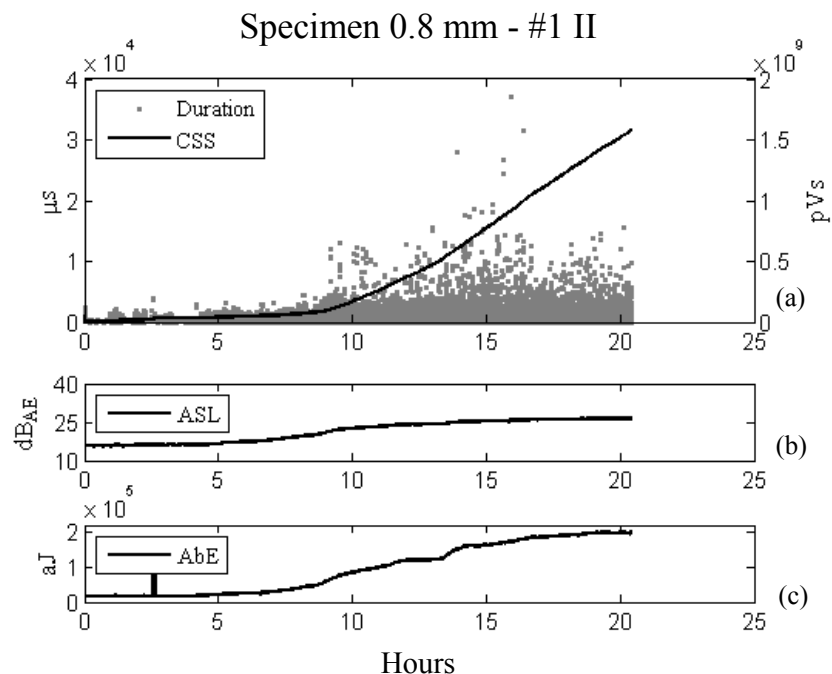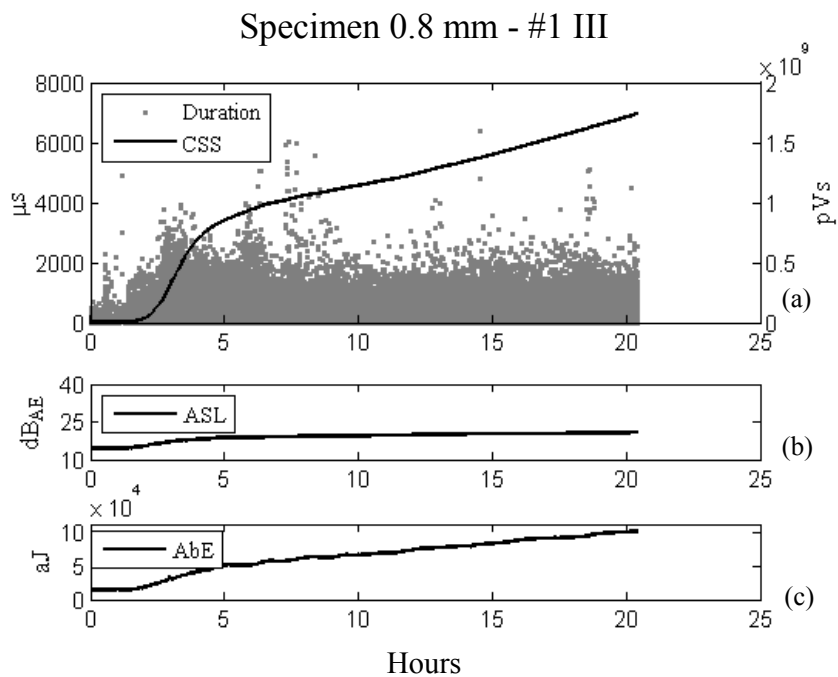
curves in Stage 1 for specimen 0.2 mm - #1 III

Figure A.4 – Cumulative signal strength (CSS) and duration (a), ASL (b) and AbE (c)

curves in Stage 1 for specimen 0.2 mm - #2 I

Figure A.5 – Cumulative signal strength (CSS) and duration (a), ASL (b) and AbE (c)
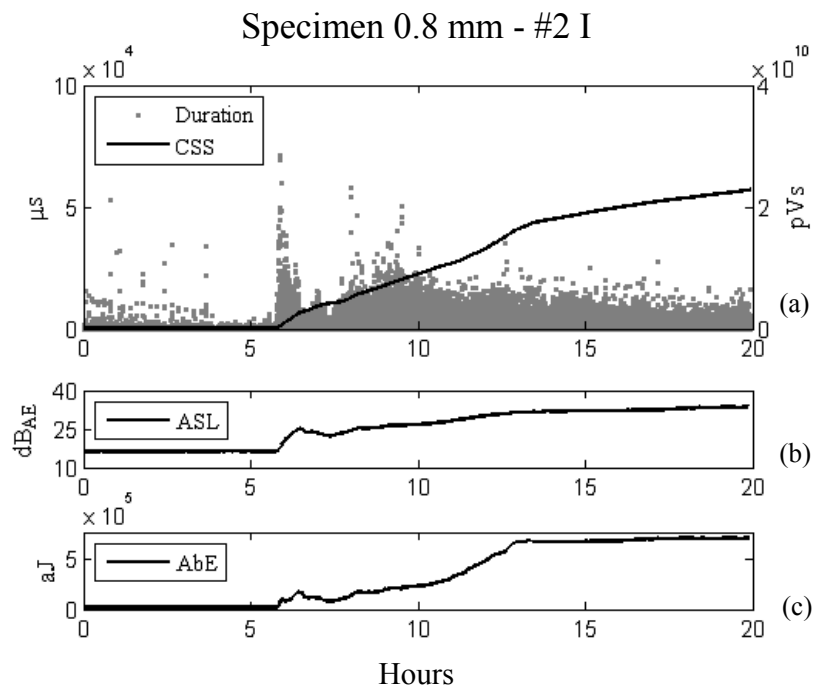
curves in Stage 1 for specimen 0.2 mm - #2 III

Figure A.6 – Cumulative signal strength (CSS) and duration (a), ASL (b) and AbE (c)

curves in Stage 1 for specimen 0.2 mm - #3 I

Figure A.7 – Cumulative signal strength (CSS) and duration (a), ASL (b) and AbE (c)

curves in Stage 1 for specimen 0.2 mm - #3 II

Specimen 0.2 mm - #3 III

Figure A.8 – Cumulative signal strength (CSS) and duration (a), ASL (b) and AbE (c)

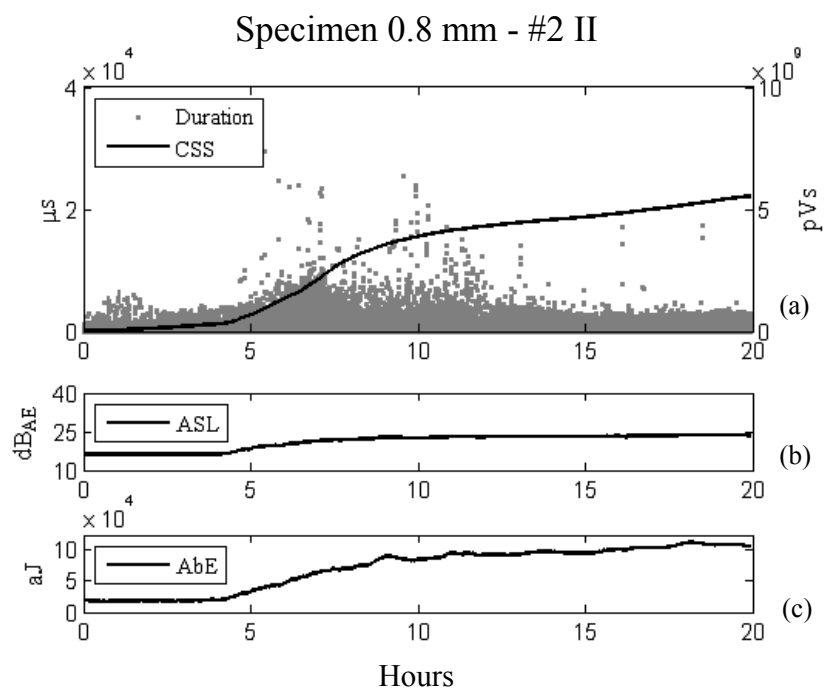curves in Stage 1 for specimen 0.2 mm - #3 III

Specimen 0.8 mm - #1 I

Figure A.9 – Cumulative signal strength (CSS) and duration (a), ASL (b) and AbE (c)

curves in Stage 1 for specimen 0.8 mm - #1 I

Figure A.10 – Cumulative signal strength (CSS) and duration (a), ASL (b) and AbE (c)

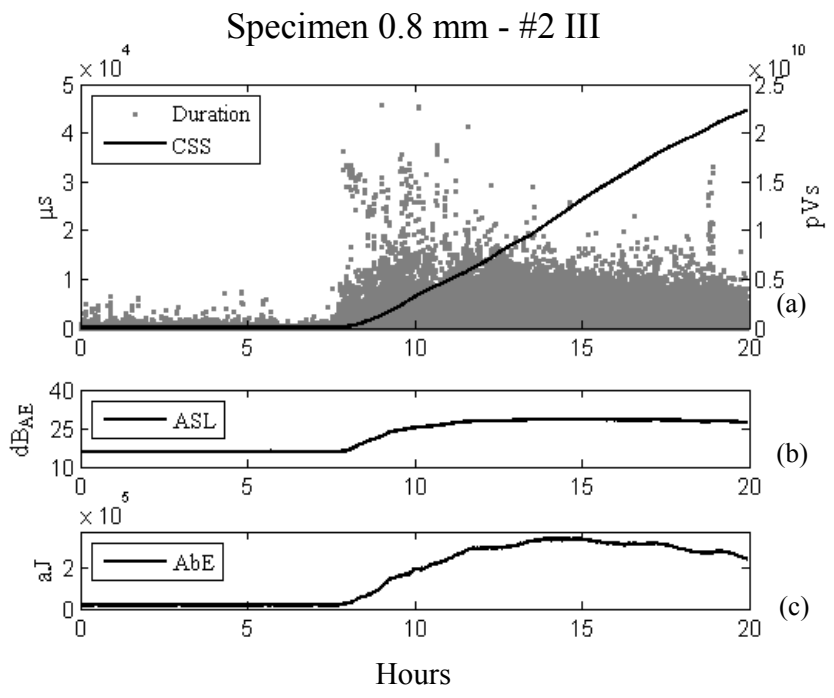curves in Stage 1 for specimen 0.8 mm - #1 II

Figure A.11 – Cumulative signal strength (CSS) and duration (a), ASL (b) and AbE (c)

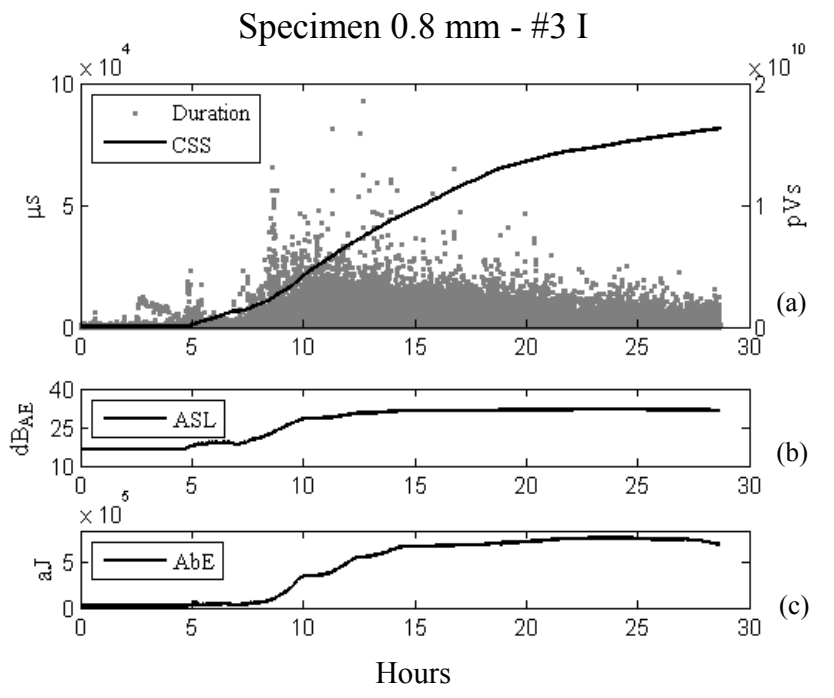curves in Stage 1 for specimen 0.8 mm - #1 III

Specimen 0.8 mm - #2 I

Figure A.12 – Cumulative signal strength (CSS) and duration (a), ASL (b) and AbE (c)

curves in Stage 1 for specimen 0.8 mm - #2 I

Specimen 0.8 mm - #2 II

Figure A.13 – Cumulative signal strength (CSS) and duration (a), ASL (b) and AbE (c)
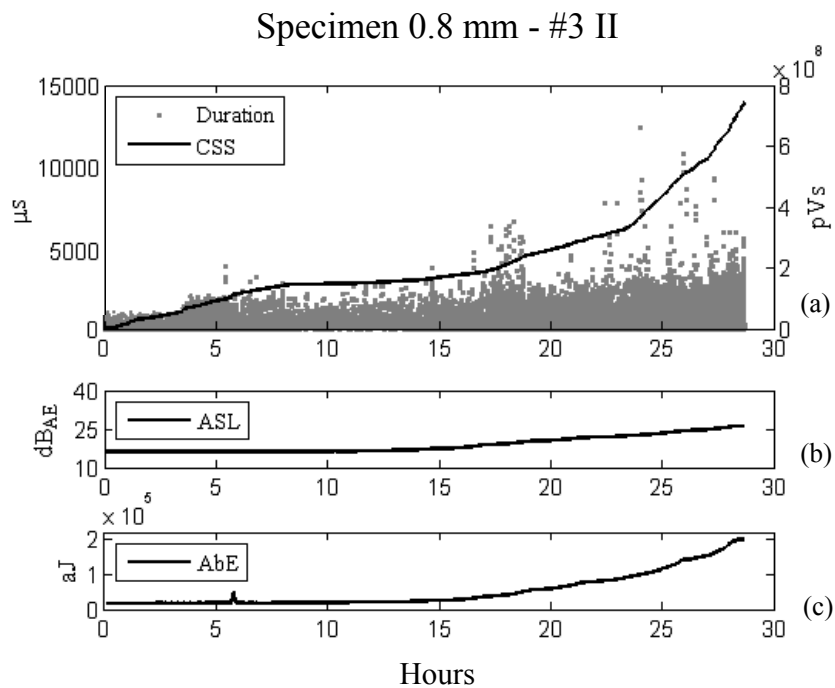
curves in Stage 1 for specimen 0.8 mm - #2 II

Figure A.14 – Cumulative signal strength (CSS) and duration (a), ASL (b) and AbE (c)

curves in Stage 1 for specimen 0.8 mm - #2 III

Figure A.15 – Cumulative signal strength (CSS) and duration (a), ASL (b) and AbE (c)

curves in Stage 1 for specimen 0.8 mm - #3 I

Specimen 0.8 mm - #3 II

Figure A.16 – Cumulative signal strength (CSS) and duration (a), ASL (b) and AbE (c)

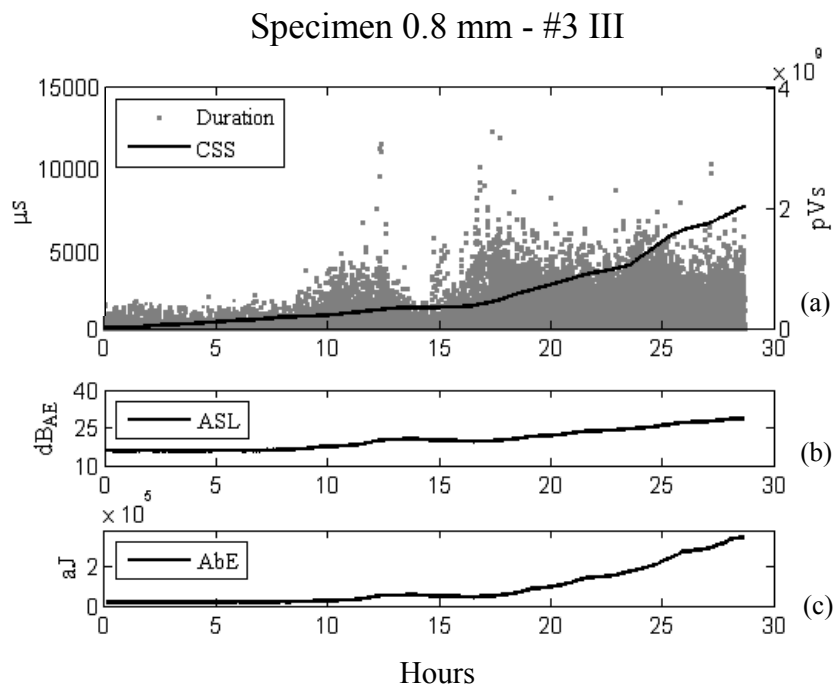curves in Stage 1 for specimen 0.8 mm - #3 II

Specimen 0.8 mm - #3 III

Figure A.17 – Cumulative signal strength (CSS) and duration (a), ASL (b) and AbE (c)
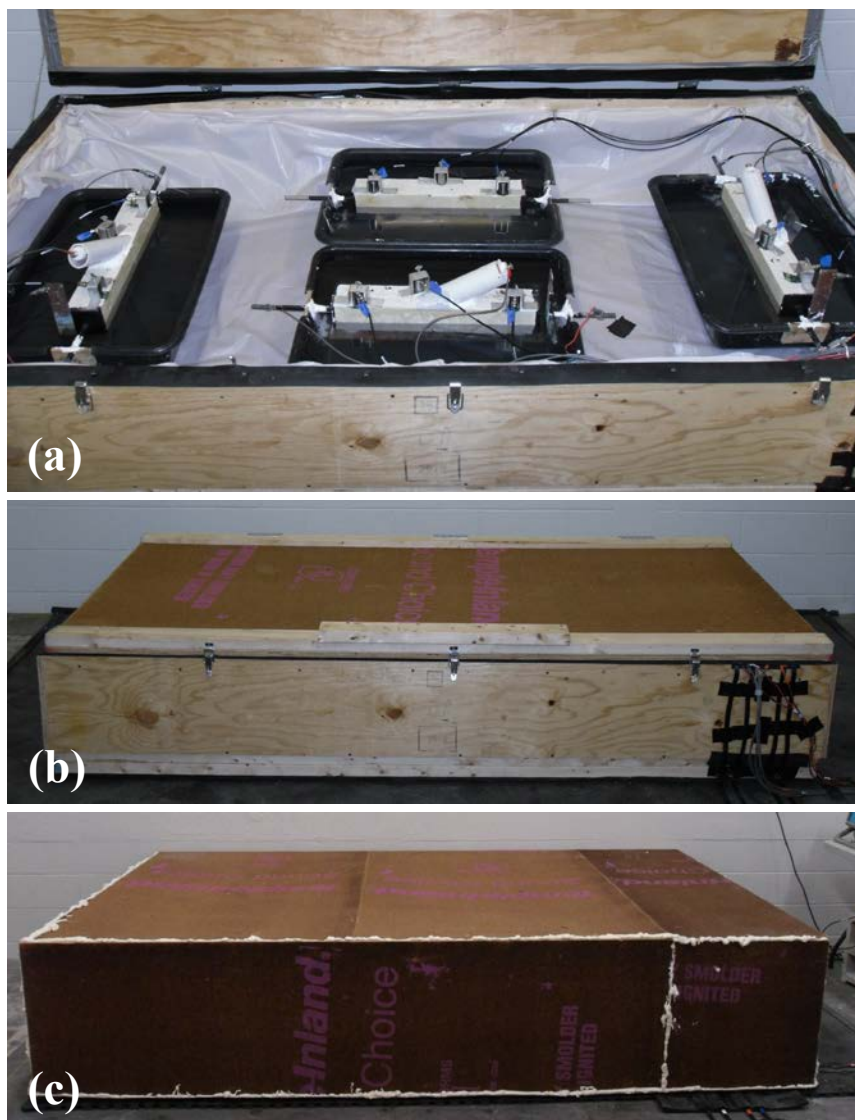
curves in Stage 1 for specimen 0.8 mm - #3 III

Figure A.18 – Soundproof boxes: during setup (a), inner box (b), outer box(c)

Figure A.19 – Mold detail. Metallic insertion for pre-notch

Specimens 0.2 mm - #1

Figure A.20 – Specimens 0.2 mm - #1 after accelerated corrosion test

Specimens 0.2 mm - #2

Figure A.21 – Specimens 0.2 mm - #2 after accelerated corrosion test
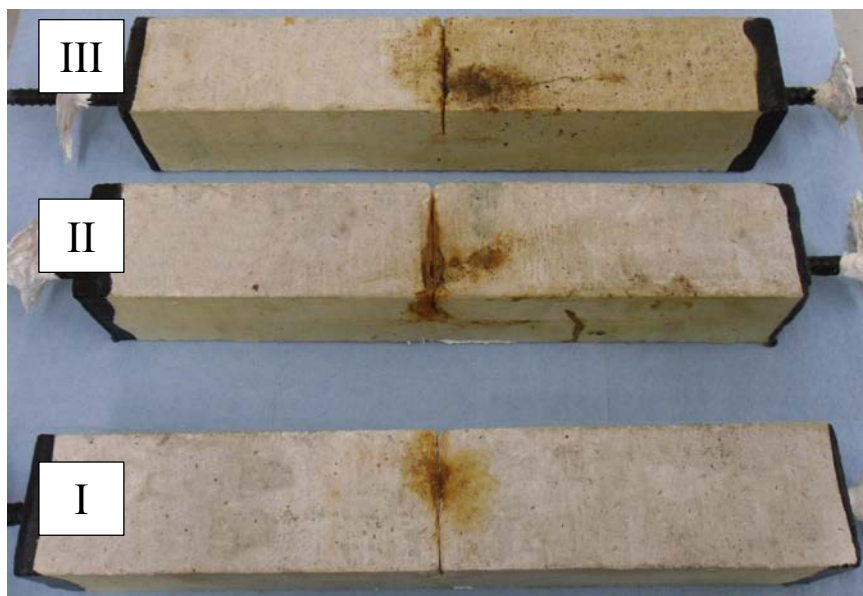
Specimens 0.2 mm - #3

Figure A.22 – Specimens 0.2 mm - #3 after accelerated corrosion test

Specimens 0.8 mm - #1

Figure A.23 – Specimens 0.8 mm - #1 after accelerated corrosion test
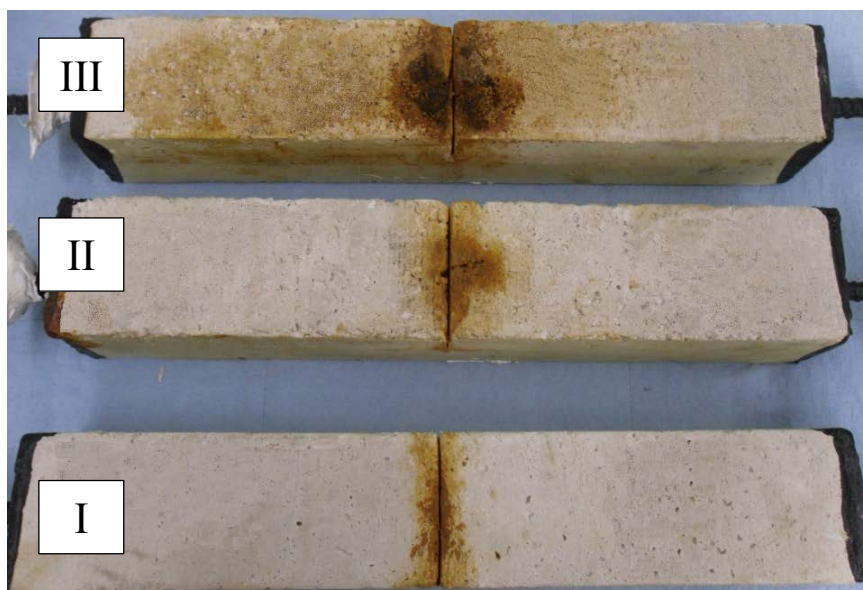
Specimens 0.8 mm - #2

Figure A.24 – Specimens 0.8 mm - #2 after accelerated corrosion test

Specimens 0.8 mm - #3

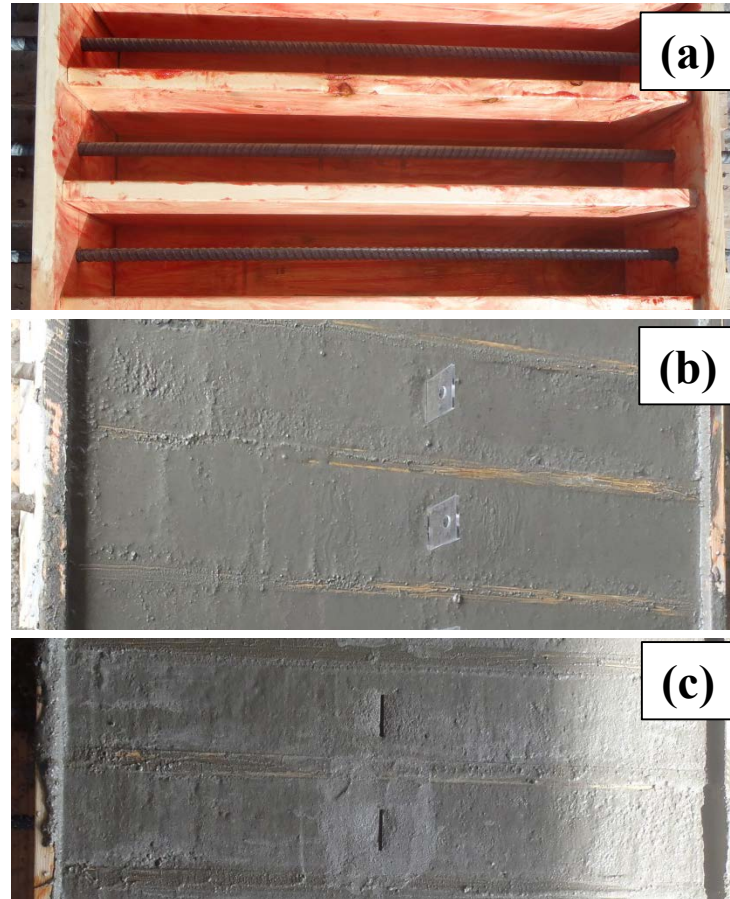Figure A.25 – Specimens 0.8 mm - #3 after accelerated corrosion test

Figure A.26 – Casting details. Empty mold treated with grease (a); plastic insertion to reduce cover thickness at mid-length (b); plastic insertion removed after few hours (c)

Figure A.27 – Plastic insertion
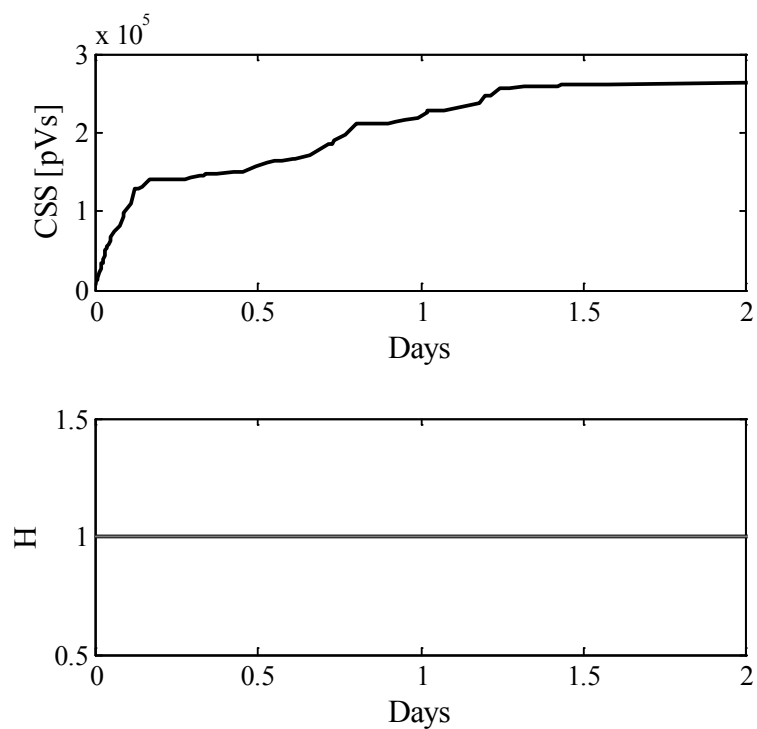
Figure A.28 – Accelerated corrosion test setup

Figure A.29 – Cumulative signal strength (CSS) and historic index (H) for specimen 1
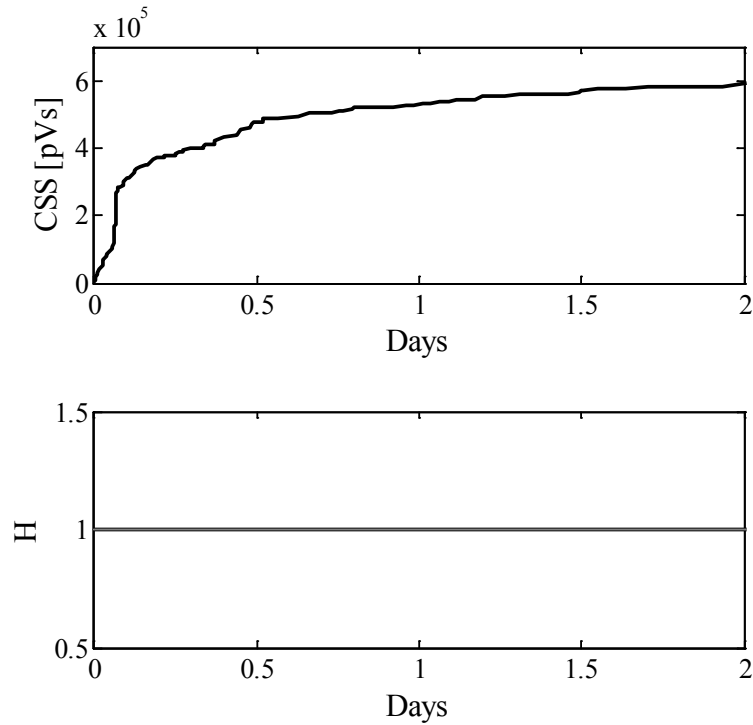during day 1 and 2

Figure A.30 – Cumulative signal strength (CSS) and historic index (H) for specimen 3 during day 1 and 2.
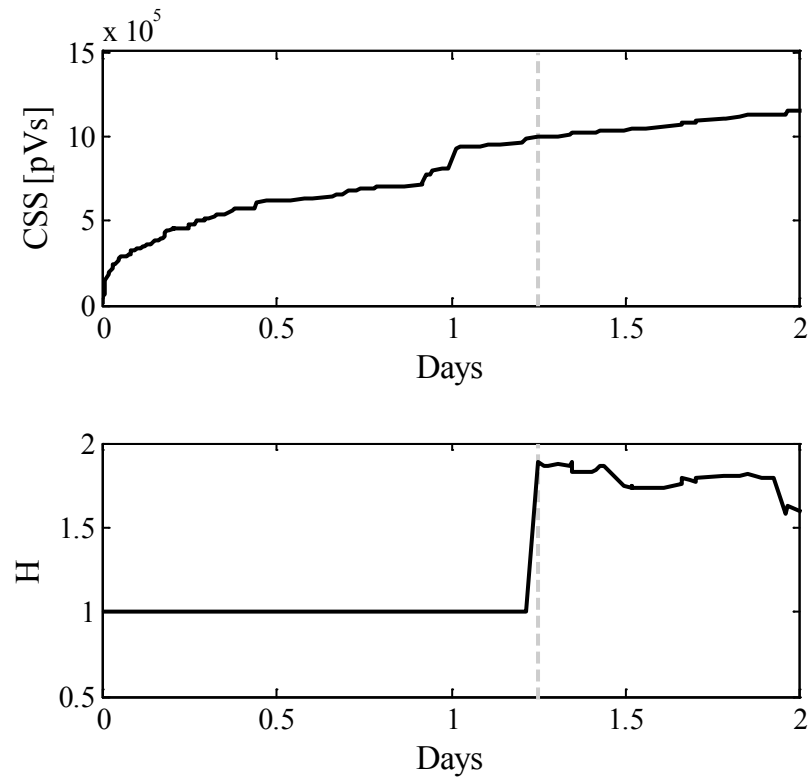

Figure A.31 – Cumulative signal strength (CSS) and historic index (H) for specimen 3 during day 1 and 2. The dashed line indicates the peak of H

Table A.1 – Half-cell potential (HCP) results for all specimens at the end of each day

	HCP [mV]					
Day	0	1	2	3	4	5
Specimen 1	-118.2	-120.9	-333.4	-433.4	-457.7	-464.7
Specimen 2	-117.6	-92.2	-231.2	-339.9	-434.3	-454.9
Specimen 3	-122.3	-127.1	-295.1	-372.9	-427.6	-440.3
Specimen 4	-115.9	-130.6	-285.1	-322.7	-439.9	-453.3

Table A.2 – Linear polarization resistance (LPR) results for all specimens at the end of each day

	LPR - R_p [Ω]					
Day	0	1	2	3	4	5
Specimen 1	2779.0	3076.0	450.9	255.0	232.4	222.9
Specimen 2	3329.0	3798.0	2046.0	523.1	266.8	254.6
Specimen 3	2461.0	2872.0	641.2	366.9	255.5	241.0
Specimen 4	2929.0	3213.0	618.5	558.0	251.6	239.5

Table A.3 – Electrochemical impedance spectroscopy (EIS) results for all specimens at the end of each day

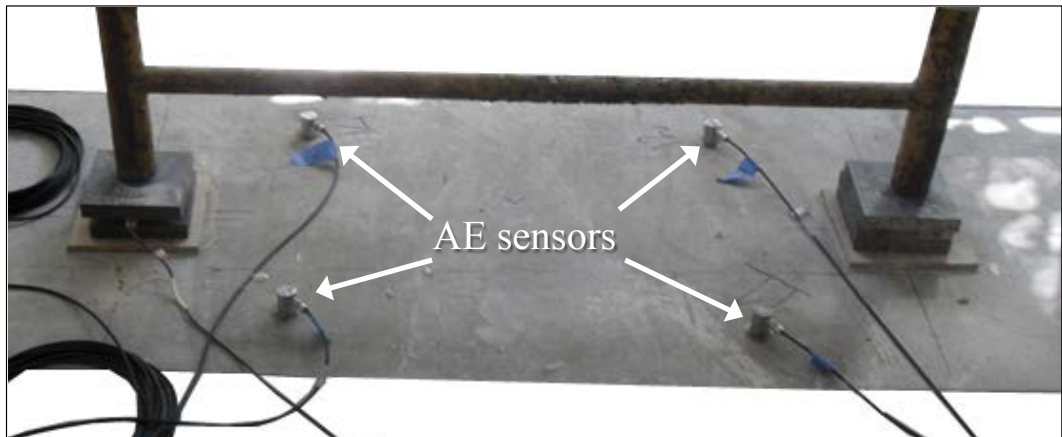|	EIS - R_s [Ω]					
Day	0	1	2	3	4	5
Specimen 1	822.6	690.7	649.4	81.4	74.0	73.7
Specimen 2	854.2	739.7	709.9	644.9	80.6	80.6
Specimen 3	839.7	705.0	80.9	81.4	74.0	74.0
Specimen 4	742.2	649.5	77.6	78.9	79.2	79.5

Figure A.32 – Saw-cutting of slab strips 1 and 2

AE sensors

Figure A.33 – Acoustic emission sensors setup

Repetition 1
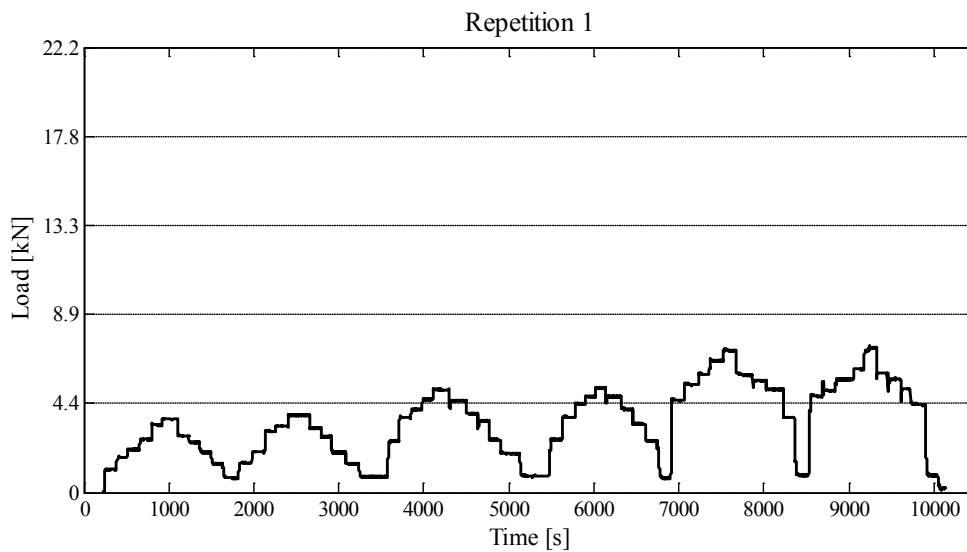

Figure A.34 – Load cycles for Repetition 1
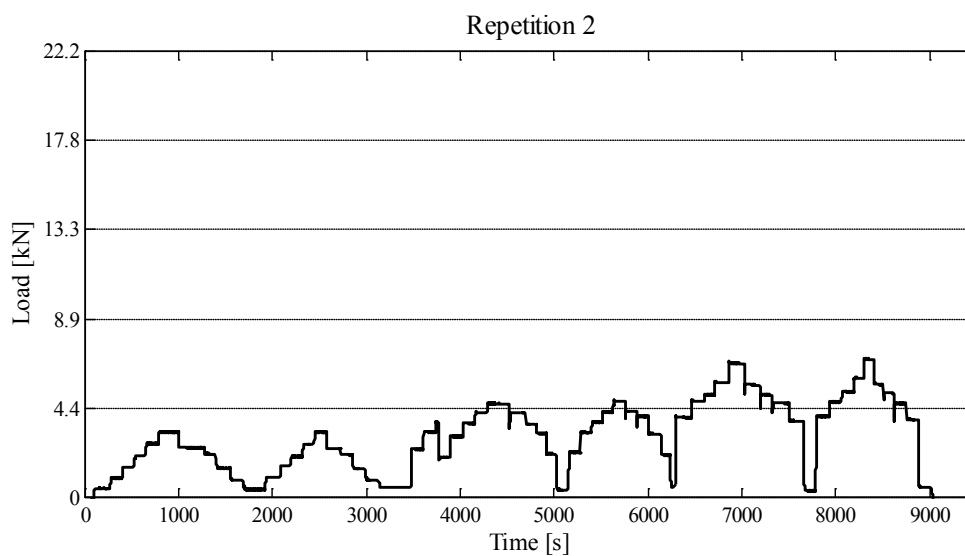
Repetition 2

Figure A.35 – Load cycles for Repetition 2
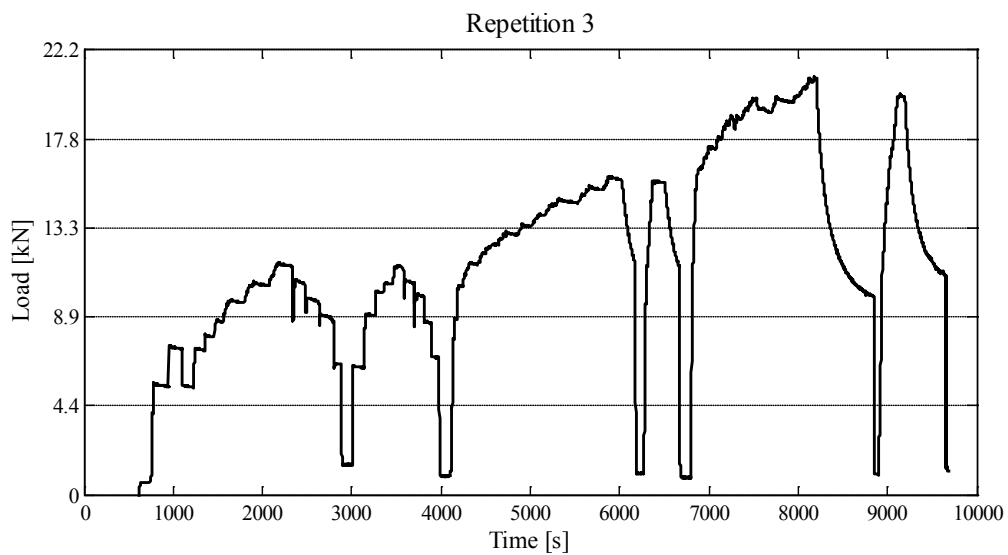
Repetition 3

Figure A.36 – Load cycles for Repetition 3
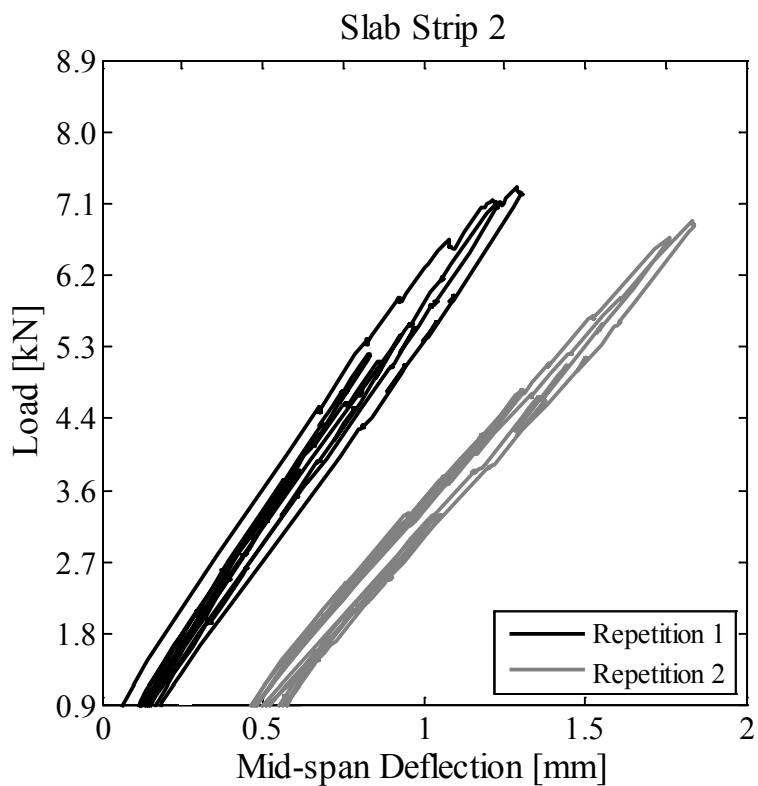
Slab Strip 2

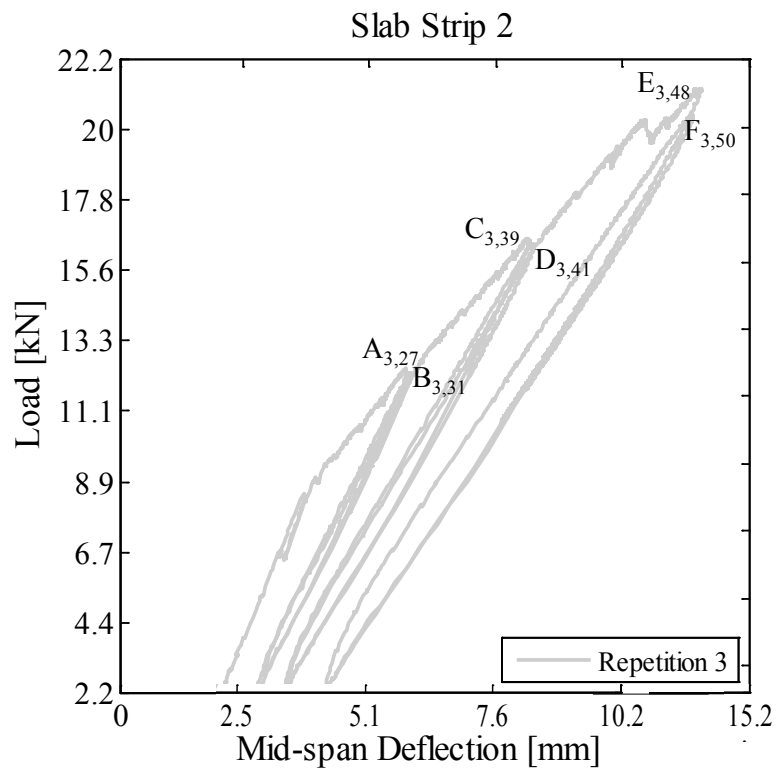Figure A.37 – Slab strip 2: load deflection curves for Repetitions 1 and 2

Figure A.38 – Slab strip 2: load deflection curves for Repetitions 1 and 2

BIBLIOGRAPHY

ACI Committee 318, [Building code requirements for structural concrete and commentary,] ACI, Farmington Hills, MI, 318-136 (2011)

ACI Committee 437, [Code requirements for load testing of concrete members of existing buildings], ACI, Farmington Hills, MI, (2012)

Allen, R.T.L., Edwards, S.C. and Shaw, J.D.N., [The repair of concrete structures,] Chapman & Hall, London, U.K., 18-22 (1993)

Andrade, C., Alonso, C., Gulikers, J., Polder, R.B., Cigna, R., Vennesland, Ø., and Salta, M., "Recommendations of RILEM TC-154-EMC: Electrochemical techniques for measuring metallic corrosion," Materials and Structures 37(273), 623-643 (2004)

Andrade, C., Alonso, C. and Molina, F.J., "Cover cracking as a function of bar corrosion: part I – experimental test," Material and Structures 26(162), 453-464 (1993)

Andrade, C. and González, J.A., "Quantitative measurements of corrosion rate of reinforcing steels embedded in concrete using polarization resistance measurements," Materials and Corrosion 29(8), 515-519 (1978)

ASCE [Report card for America's infrastructure,] American Society of Civil Engineers, Reston, VA, 73-81 (2009)

Assouli, B., Simescu, F., Debicki, G., and Idrissi, H. "Detection and identification of concrete cracking during corrosion of reinforced concrete by acoustic emission coupled to the electrochemical techniques," NDT&E International 38, 682-689 (2005)

ASTM Standard C876, "Standard test method for half-cell potentials of uncoated reinforcing steel in concrete," ASTM International, West Conshohocken, PA, (2009)

ASTM Standard E1316, "Standard terminology for nondestructive examinations," ASTM International, West Conshohocken, PA, (2010)

ASTM Standard E2478 "Standard practice for determining damage-based design criteria for fiberglass reinforced plastic (FRP) materials using acoustic emission," ASTM International, West Conshohocken, PA, (2006)

ASTM Standard G59, "Standard test method for conducting potentiodynamic polarization resistance measurements," ASTM International, West Conshohocken, PA, (2009)

89

ASTM Standard G102, "Standard practice for calculation of corrosion rates and related information from electrochemical measurements," ASTM International, West Conshohocken, PA, (2004)

ASTM Standard G106 "Standard practice for verification of algorithm and equipment for electrochemical impedance measurements," ASTM International, West Conshohocken, PA, (2004)

Ballim, Y. and Reid, J.C., "Reinforcement corrosion and the deflection of RC beams – an experimental critique of current test methods," Cement & Concrete Composites 25(6), 625–632 (2003)

Browne, R.D., "Mechanism of corrosion of steel in concrete in relation to design, inspection and repairs of offshore and coastal structures," ACI SP 65(11), 169–204 (1980)

Budynas, R.G., [Advanced strength and applied stress analysis, second edition,] McGraw Hill, 509-513 (1998)

Colombo, S., Forde, M.C., Main, I.G. and Shigeishi, M., "Predicting the ultimate bending capacity of concrete beams from the relaxation ratio analysis of AE signals," Construction and Building Materials, 19, 746-754 (2005)

Darwin, D., Manning, D.G., Hognestad, E., Beeby, A.W., Rice, P.F. and Ghowrwal, A.Q., "Debate: crack width, cover, and corrosion," Concrete International 7(5), 20-35 (1985)

De Luca, A., Jawaheri Zadeh, H. and Nanni, A., "Assessment of the performance of RC strips by in-situ load testing," ACI Structural Journal, (2012, in print)

Fowler, T.J., Blessing, J.A., Conlisk, P.J. and Swanson, T.L., "The MONPAC system," Journal of Acoustic Emission, 8(3), 1-8 (1989)

Fregonese, M., Idrissi, H., Mazille, H., Renaud, L. and Cètre, Y., "Monitoring pitting corrosion of 304L and 316L austenitic stainless steels by acoustic emission: influence of the pit morphology," Proc. European Corrosion Congress 99, Wernicke, H.J., Aachen, GER (1999)

Gamry Instruments Inc., [Reference 600^{TM} – potentiostat / galvanostat / ZRA – operator's manual,] Gamry Instruments Inc., Warminster, PA (2011)

Godínez-Azcuaga, V.F., Farmer, J., Ziehl, P.H., Giurgiutiu, V., Nanni, A. and Inman, D.J., "Status in the development of self-powered wireless sensor node for structural health monitoring and prognosis," Proc. SPIE Smart Structures and Materials + Nondestructive Evaluation and Health Monitoring, San Diego, CA, (2012).

Golaski, L., Gebski, P. and Ono, K., "Diagnostics of reinforced concrete bridges by acoustic emission," Journal of Acoustic Emission, 20, 83-98 (2002)

Han, S.H., Lee, W.J., Cho, H.D. and Kim, D.G., "Crack source location technique for plain concrete beam using acoustic emission," Journal of Korean Concrete Institute 13(2), 107-113, (2001)

Hearn, S.W., and Shield, C.K., "Acoustic emission monitoring as a nondestructive testing technique in reinforced concrete," ACI Materials Journal, 94(6), 510-519 (1997)

Higgins, D.D., "The effect of some test variables on chloride profiles," RILEM International Workshop on Chloride Penetration into Concrete, Paris, 1995

Hope, B., Page, J.A. and Ip, A.K.C., "Corrosion rates of steel in concrete," Cement and Concrete Research 16(5), 771–781 (1986)

Idrissi, H. and Liman, A., "Study and characterization by acoustic emission and electrochemical measurements of concrete deterioration caused by reinforcement steel corrosion," NDT&E International 36(8), 563-569 (2003)

Kim, Y.P., Fregonese, M., and Feron, D., "Ability of acoustic emission technique for detection and monitoring of crevice corrosion on 304L austenitic stainless steel," NDT&E International 36(8), 553-562 (2003)

Lee, C., Bonacci, J.F., Thomas, M.D.A., Maalej, M., Khajehpour, S., Hearn, N., Pantazopoulou, S. and Sheikh, S. "Accelerated corrosion and repair of reinforced concrete columns using carbon fiber reinforced polymer sheets," Canadian Journal of Civil Engineering, 27(5), 941-948 (2000)

Li, Z., Li, F., Zdunek, A., Landis, E. and Shah, S., "Application of acoustic emission to detection of reinforcing steel corrosion in concrete," ACI Materials Journal 95(1), 68-76 (1998)

Liu, Z., "Evaluation of reinforced concrete beams using cyclic load test, acoustic emission and acousto-ultrasonics," University of South Carolina, Columbia, SC, (2007)

Liu, Z. and Ziehl, P.H., "Evaluation of reinforced concrete beam specimens with acoustic emission and cyclic load test methods," ACI Structural Journal, 106(3), 288-299 (2009)

Loreto, G., Di Benedetti, M. and Nanni, A., "Durability of reinforced concrete in marine environmental: a simplified model for service life prediction," International Journal of 3R's (2011, in print)

Lovejoy, S.C., "Acoustic emission testing of in-service conventionally reinforced concrete deck girder superstructures on highway bridges", Final Report SPR 633, Oregon Department of Transportation Bridge and Engineering Section, (2008)

Lovejoy, S.C., "Acoustic emission testing of beams to simulate SHM of vintage reinforced concrete deck girder highway bridges," Structural Health Monitoring, 7(4), 329-345 (2008)

Montgomery, D.C. and Runger, G.C., [Applied statistics and probability for engineers - 3rd ed.,] John Wiley & Sons, Inc., New York, NY, 384-386 (2003)

Melchers, R.E. and Li, C.Q., "Phenomenological modeling of reinforcement corrosion in marine environments," ACI Materials Journal 103(1), 25-32 (2006)

Nygaard, P.V. and Geiker, M.R., "A method for measuring the chloride threshold level required to initiate reinforcement corrosion in concrete," Materials and Structures 38, 489-494 (2005)

Ohtsu, M., "Acoustic emission characteristics in concrete and diagnostic applications," Journal of Acoustic Emission, 6(2), 99-108 (1987)

Ohtsu, M. and Yuyama, S., "Recommended practice for in situ monitoring of concrete structures by acoustic emission," NDIS 2421, Japanese Society for Nondestructive Inspection, (2000)

Ohtsu, M., Uchida, M., Okamoto, T., and Yuyama, S., "Damage assessment of reinforced concrete beams qualified by acoustic emission," ACI Structural Journal, 99(4), 411-417 (2002)

Ohtsu, M. and Tomoda, Y., "Phenomenological model of corrosion process in reinforced concrete identified by acoustic emission," ACI Materials Journal 105(2), 194-199 (2008)

Otieno, M.B., Alexander, M.G. and Beushausen, H.D., "Corrosion in cracked and uncracked concrete – influence of crack width, concrete quality and crack reopening," Magazine of Concrete Research 62(6), 393-404 (2010)

Physical Acoustic Corporation, [R6I-AST sensor – integral preamplifier acoustic emission sensor,] Physical Acoustic Corporation, Princeton Junction, NJ, (2005)

Physical Acoustic Corporation, [Sensor Highway – II, user's manual,] Physical Acoustic Corporation, Princeton Junction, NJ, 22-23 (2009)

Physical Acoustic Corporation, [R6D sensor – general purpose differential sensor,] Physical Acoustic Corporation, Princeton Junction, NJ, (2011)

Proust, A., Mazille, H., Fleischmann, P. and Rothea, R., "Characterization by AE technique of emissive phenomena during stress corrosion cracking of stainless steels," Journal of Acoustic Emission 19, 19229-19240 (2001)

Ridge, A.R. and Ziehl, P.H., "Evaluation of strengthened reinforced concrete beams: cyclic load test and acoustic emission methods," ACI Structural Journal, 103(6), 832-841 (2006)

Shalon, R. and Raphael, M., "Influence of sea water on corrosion of steel reinforcement," Journal of the American Concrete Institute 55, 1251-1268 (1959)

Yoon, D.J., Weiss, W.J. and Shah, S., "Assessing damage in corroded reinforced concrete using acoustic emission," Journal of Engineering Mechanics 126(3), 273-283 (2000)

Yuan, Y., Ji, Y. and Shah, S.P., "Comparison of two accelerated corrosion techniques for concrete structures," ACI Structural Journal 104(3), 344-347 (2007)

Yuyama, S., Okamoto, T., Shigeishi, M., Ohtsu, M., and Kishi T., "A proposed standard for evaluating structural integrity of reinforced concrete beams by acoustic emission," Acoustic Emission: Standards and Technology Update, ASTM STP 1353, S. J. Vahaviolos, Ed., ASTM, West Conshohocken, PA, 25-40 (1999)

Yuyama, S. and Nishida, T., "Acoustic emission evaluation of corrosion damages in buried pipes of refinery," Progress in Acoustic Emission 11, 197-204 (2002)

Ziehl, P.H. and Fowler, T.J., "Fiber reinforced polymer vessel design with a damage approach," Journal of Composite Structures 61, 395-411 (2003)

Ziehl, P.H., Galati, N., Nanni, A. and Tumialan, J.G., "In-situ evaluation of two concrete slab systems. II: evaluation criteria and outcomes," ASCE Journal of Performance of Constructed Facilities 22(4), 217-227 (2008)